

# Paleoceanography and Paleoclimatology

## RESEARCH ARTICLE

10.1029/2019PA003713

### Key Points:

- We present a new record of pCO<sub>2</sub> across the MECO, from boron isotopes in foraminifera from multiple ocean drilling sites
- Incorporating carbon cycle modeling, our data indicate pCO<sub>2</sub> rise of about two thirds of a doubling across the event
- pCO<sub>2</sub> change during the MECO onset warming was limited, indicating heightened climate sensitivity or a nonthermal component to δ<sup>18</sup>O change

### Supporting Information:

- Supporting Information S1
- Tables S1–S3

### Correspondence to:

M. J. Henehan and K. M. Edgar,  
michael.henehan@gfz-potsdam.de;  
k.m.edgar@bham.ac.uk

### Citation:

Henehan, M. J., Edgar, K. M., Foster, G. L., Penman, D. E., Hull, P. M., Greenop, R., et al. (2020). Revisiting the Middle Eocene Climatic Optimum “Carbon Cycle Conundrum” with new estimates of atmospheric pCO<sub>2</sub> from boron isotopes. *Paleoceanography and Paleoclimatology*, 35, e2019PA003713. <https://doi.org/10.1029/2019PA003713>

Received 4 JUL 2019

Accepted 26 FEB 2020

Accepted article online 9 MAR 2020

Corrected 17 JUN 2020

This article was corrected on 17 JUN 2020. See the end of the full text for details.

### Author Contributions:

**Conceptualization:** Michael J. Henehan, Kirsty M. Edgar, Gavin L. Foster, Donald E. Penman, Pincelli M. Hull, Rosanna Greenop, Eleni Anagnostou, Paul N. Pearson

**Data curation:** Michael J. Henehan, Kirsty M. Edgar  
(continued)

©2020. The Authors.

This is an open access article under the terms of the Creative Commons Attribution License, which permits use, distribution and reproduction in any medium, provided the original work is properly cited.

## Revisiting the Middle Eocene Climatic Optimum “Carbon Cycle Conundrum” With New Estimates of Atmospheric pCO<sub>2</sub> From Boron Isotopes

Michael J. Henehan<sup>1,2,3</sup> , Kirsty M. Edgar<sup>4</sup> , Gavin L. Foster<sup>1</sup> , Donald E. Penman<sup>3</sup> , Pincelli M. Hull<sup>3</sup>, Rosanna Greenop<sup>5</sup> , Eleni Anagnostou<sup>6</sup> , and Paul N. Pearson<sup>7</sup>

<sup>1</sup>School of Ocean and Earth Science, National Oceanography Centre Southampton, University of Southampton, Southampton, UK, <sup>2</sup>GFZ German Research Centre for Geosciences, Potsdam, Germany, <sup>3</sup>Department of Geology and Geophysics, Yale University, New Haven, CT, USA, <sup>4</sup>School of Geography, Earth and Environmental Sciences, University of Birmingham, Birmingham, UK, <sup>5</sup>Department of Earth Sciences, Irvine Building, University of St. Andrews, St. Andrews, UK, <sup>6</sup>GEOMAR Helmholtz Center for Ocean Research Kiel, Kiel, Germany, <sup>7</sup>School of Earth and Ocean Sciences, Cardiff University, Cardiff, UK

**Abstract** The Middle Eocene Climatic Optimum (MECO) was a gradual warming event and carbon cycle perturbation that occurred between 40.5 and 40.1 Ma. A number of characteristics, including greater-than-expected deep-sea carbonate dissolution, a lack of globally coherent negative δ<sup>13</sup>C excursion in marine carbonates, a duration longer than the characteristic timescale of carbon cycle recovery, and the absence of a clear trigger mechanism, challenge our current understanding of the Earth system and its regulatory feedbacks. This makes the MECO one of the most enigmatic events in the Cenozoic, dubbed a middle Eocene “carbon cycle conundrum.” Here we use boron isotopes in planktic foraminifera to better constrain pCO<sub>2</sub> changes over the event. Over the MECO itself, we find that pCO<sub>2</sub> rose by only 0.55–0.75 doublings, thus requiring a much more modest carbon injection than previously indicated by the alkenone δ<sup>13</sup>C-pCO<sub>2</sub> proxy. In addition, this rise in pCO<sub>2</sub> was focused around the peak of the 400 kyr warming trend. Before this, considerable global carbonate δ<sup>18</sup>O change was asynchronous with any coherent ocean pH (and hence pCO<sub>2</sub>) excursion. This finding suggests that middle Eocene climate (and perhaps a nascent cryosphere) was highly sensitive to small changes in radiative forcing.

**Plain Language Summary** Geoscientists often look to periods of global warming in the geological past to understand how the Earth responds to input of atmospheric CO<sub>2</sub>. However, during the Middle Eocene Climatic Optimum (or MECO) 40 million years ago, the Earth did not respond in the way one would expect, given what we know from these earlier warming events. The MECO poses a number of puzzles for geoscientists relating to what caused it and why the Earth system responded in the way it did. Before we can hope to answer these questions, however, we need to know what atmospheric CO<sub>2</sub> levels were in the middle Eocene and how much they changed over the MECO event. Here we use boron isotope ratios in fossil plankton shells to tell us how ocean pH (which predominantly reflects CO<sub>2</sub> levels) changed over the MECO. We show that relatively little change in CO<sub>2</sub> at this time were associated with large-scale changes in climate. This suggests that during the Eocene, when CO<sub>2</sub> levels were similar to those likely to be reached by the end of this century, the Earth's climate (and possibly ice sheets) was very sensitive to minor disturbances.

## 1. Introduction

The Middle Eocene Climatic Optimum (MECO; ~40.1–40.5 Ma) was a global warming event during which marine bulk and benthic carbonate δ<sup>18</sup>O values steadily declined by roughly 1‰ in over ~400 kyr, usually interpreted as 3–6 °C of global temperature rise (Bohaty et al., 2009; Bohaty & Zachos, 2003). While sometimes referred to as a hyperthermal event (e.g., Arreguín-Rodríguez et al., 2016; Pomar et al., 2017), the MECO differs fundamentally from the true hyperthermal events earlier in the Paleogene, such as the Paleocene-Eocene Thermal Maximum (PETM, ~56 Ma) or Eocene Thermal Maximum 2 (ETM2; ~53.7 Ma). First, these hyperthermal events were rapid in their onset (<10 kyr; Kirtland Turner et al., 2017) and were followed by a gradual return to roughly pre-event temperatures as the silicate weathering feedback drew down atmospheric CO<sub>2</sub> (e.g., Kelly et al., 2005; Penman, 2016;

**Formal analysis:** Michael J. Henehan, Kirsty M. Edgar, Donald E. Penman, Eleni Anagnostou  
**Funding acquisition:** Gavin L. Foster, Paul N. Pearson  
**Investigation:** Michael J. Henehan, Kirsty M. Edgar, Donald E. Penman  
**Resources:** Gavin L. Foster  
**Software:** Michael J. Henehan, Gavin L. Foster, Donald E. Penman  
**Supervision:** Gavin L. Foster, Pincelli M. Hull  
**Visualization:** Michael J. Henehan  
**Writing - original draft:** Michael J. Henehan, Kirsty M. Edgar  
**Writing - review & editing:** Michael J. Henehan, Kirsty M. Edgar, Gavin L. Foster, Donald E. Penman, Pincelli M. Hull, Rosanna Greenop, Eleni Anagnostou, Paul N. Pearson

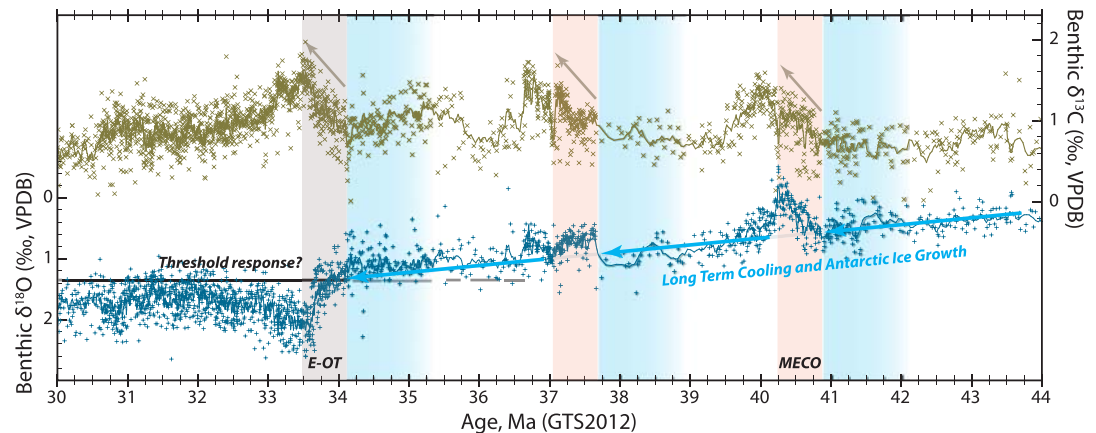


**Figure 1.** Repeating patterns in  $\delta^{13}\text{C}$  and  $\delta^{18}\text{O}$  during the middle-late Eocene and early Oligocene are evident in the benthic foraminiferal compilation of Cramer et al. (2009), here shown adjusted to the Geological Timescale 2012 (GTS2012; Gradstein et al., 2012). In each case, excursions toward higher benthic foraminiferal  $\delta^{13}\text{C}$  coincide with instances where  $\delta^{18}\text{O}$  changes diverge from the underlying trend of cooling and ice growth in the middle-late Eocene. “E-OT” as marked in the gray band denotes the Eocene-Oligocene transition.

Penman et al., 2016; Zachos et al., 2005), whereas the MECO saw a steady decline in carbonate  $\delta^{18}\text{O}$  values over several 100 kyr (interpreted as gradual warming), followed by a rapid return to pre-event conditions (Bohaty et al., 2009). A second important distinction is that the earlier hyperthermal events are clearly marked by sharp drops in  $\delta^{13}\text{C}$  that are expressed globally in both marine  $\text{CaCO}_3$  and terrestrial records (e.g., Abels et al., 2012; Kennett & Stott, 1991; Koch et al., 1992; Westerhold, Röhl, Donner, Frederichs, et al., 2018; Westerhold, Röhl, Donner, & Zachos, 2018; Zachos et al., 2005). These carbon isotope excursions (or CIEs) are thought to be manifestations of rapid injections of isotopically light C into the Earth system, perhaps from volcanic sills intruding into organic rich sediments (Gutjahr et al., 2017; Storey et al., 2007; Svensen et al., 2004) and/or the release of seafloor methane clathrates (Dickens et al., 1995). A small negative  $\delta^{13}\text{C}$  excursion is observed at the peak of the 400 kyr MECO warming trend in most marine records but is not uniformly expressed (e.g., at ODP Site 1263; Bohaty et al., 2009) and appears in some cases to lag behind minimum  $\delta^{18}\text{O}$  values (e.g., at ODP Site 702; Bohaty et al., 2009). Furthermore, during the first few 100 kyr of warming, patterns of carbon isotope change are inconsistent between sites: global bulk carbonate  $\delta^{13}\text{C}$  values display inverse trends in each hemisphere, with progressively lighter  $\delta^{13}\text{C}$  during MECO warming in northern latitudes, minimal  $\delta^{13}\text{C}$  change in the tropics, and progressively heavier  $\delta^{13}\text{C}$  during warming toward the southern high latitudes (Bohaty et al., 2009). Thus, unlike the hyperthermal events, the MECO is difficult to attribute to a simple, rapid injection of exogenously isotopically light carbon.

One characteristic that the MECO perhaps unexpectedly shares with the hyperthermal events is extensive dissolution of deep-sea sediments, representing a shoaling of the carbonate compensation depth (CCD; Bohaty et al., 2009; Bohaty & Zachos, 2003). During the hyperthermal events, this carbonate dissolution occurred in response to  $\text{CO}_2$  being injected into the ocean-atmosphere system faster than the capacity of silicate weathering on land to draw it down and input alkalinity to the ocean (see, e.g., Berner et al., 1983; Colbourn et al., 2015; Kirtland Turner et al., 2017). MECO warming, however, was nearly an order of magnitude slower than the PETM, and as such, chemical weathering feedbacks should have kept pace with warming (Colbourn et al., 2015; Sluijs et al., 2013). This would be expected to have driven a deepening of the CCD instead of the  $\sim 1$  km shoaling observed. Moreover, at the MECO, there is little signal of a “carbonate overshoot” following the event (Bohaty et al., 2009; Sluijs et al., 2013), as is seen after the PETM (Penman et al., 2016). Since these carbonate overshoots are thought to reflect the Earth’s silicate weathering feedback drawing down injected  $\text{CO}_2$ , the absence of any such event after the MECO might suggest either (a) a relatively small addition of  $\text{CO}_2$  and/or (b) a weakened silicate weathering response to  $\text{CO}_2$  rise during this interval. The latter scenario is favored by a recent study by van der Ploeg et al. (2018), who observed a

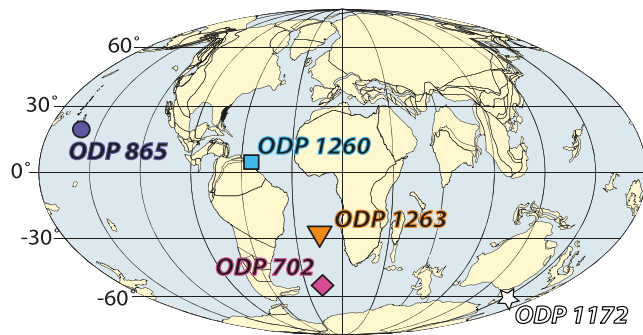


**Figure 2.** Locations of our study sites (colored markers) on a continental reconstruction from ~40 Ma from [www.ods.n.de](http://www.ods.n.de) (Hay et al., 1999). The location of ODP Site 1172 (where alkenone-based  $pCO_2$  reconstructions from Bijl et al., 2010, were derived) is also marked as a white star.

reduction in the  $^{187}Os/^{188}Os$  composition of seawater over the MECO. While this observation could be consistent with (a) a rise in hydrothermal activity, (b) an increase in weathering of mafic silicate rocks, or (c) a decrease in weathering of felsic radiogenic continental rocks, a reduction in continental weathering is more easily reconciled with deep-sea carbonate dissolution. Consequently, van der Ploeg et al. hypothesize that after tens of millions of years of intense weathering under greenhouse Eocene climates, Earth's silicate weathering feedback was no longer strong enough to buffer a carbon cycle imbalance at the MECO (van der Ploeg et al., 2018).

While a weakened silicate weathering feedback is an intriguing hypothesis, it does pose its own questions. First, the idea that the baseline middle Eocene earth surface was no longer as readily weatherable is based on Li isotopes measured in foraminifera (Misra & Froelich, 2012). However, even leaving potential non-seawater controls on foraminiferal  $\delta^7Li$  aside (Roberts et al., 2018; Vigier et al., 2015), there is more than one possible solution that could have resulted in light seawater  $\delta^7Li$ , including sustained high rates of regolith chemical weathering and soil production (Vigier & Godd eris, 2015). Second, one of the most pronounced features of the MECO is a rapid (10s of kyr) drop in temperatures after the peak of the warming trend, which would indicate some unexplained reactivation of the silicate weathering feedback after million years of hypothesized gradual decline.

Another outstanding question surrounding the MECO is that of causality. The long, drawn-out nature of the MECO warming might suggest a sustained  $CO_2$  release, and hence perhaps a volcanic source, by analogy to the several 100 kyr-long late Maastrichtian warming event (LMWE) thought to have been caused by Deccan outgassing (e.g., Barnet et al., 2018; Henehan, Hull et al., 2016). A number of potential sources of volcanic  $CO_2$  at the MECO exist (summarized in van der Ploeg et al., 2018), but the synchronicity of any one volcanic degassing event with MECO warming is yet to be demonstrated. Besides this, the coincidence of the MECO with a 2.4 Myr very long eccentricity cycle minimum (Westerhold & R ohl, 2013) might implicate an orbital trigger instead. These long eccentricity 2.4 Myr cycles have recently been shown to coincide with numerous excursions in  $\delta^{13}C$  and  $\delta^{18}O$  during the early Cenozoic (Barnet et al., 2019; Kocken et al., 2019), and carbon cycle models have been able to reproduce significant changes in the Earth's carbon cycle due to oscillating carbon reservoirs on these timescales, inducing sizeable changes in  $pCO_2$  and the CCD (Kocken et al., 2019). Observed cyclical changes in the Pacific CCD in the Eocene (Lyle et al., 2005; P alike et al., 2012) appear to have a roughly 2.4 Myr periodicity (Kocken et al., 2019), and the MECO follows the most pronounced and extreme of these periodic carbonate accumulation events (CAEs) (Lyle et al., 2005). It is possible that a combination of volcanic outgassing and a favorable orbital configuration may have been key to the amplification of the MECO as a major carbon cycle perturbation, as has been suggested for the PETM and LMWE (Barnet et al., 2019). Alternatively, it is also conceivable that orbital configuration alone could have independently induced carbon cycle changes (as with the Early-Late Paleocene Event; Barnet et al., 2019), perhaps through changing rainfall patterns and hence silicate weathering intensity (Westerhold & R ohl, 2013). Indeed, repeating patterns in carbonate  $\delta^{13}C$  and  $\delta^{18}O$  values (Figure 1) might favor some such internally modulated, pseudo-cyclic carbon cycle imbalance rather than a stochastic carbon injection from a volcanic source.

Constraining atmospheric  $pCO_2$  across the MECO is central to understanding both the causal drivers of the MECO and the Earth system's enigmatic response to the event. The only published  $pCO_2$  reconstruction over the MECO to date is that of Bijl et al. (2010), derived from alkenone  $\delta^{13}C$ . While undoubtedly pioneering, the record poses even more questions of its own, in that taken at face value it indicates several high-amplitude fluctuations on the order of several thousand  $\mu atm$  of  $CO_2$  over the MECO, asynchronous with a near-linear decline in  $\delta^{18}O$ . This would appear incongruous in the context of background  $pCO_2$  levels in the middle Eocene reconstructed from boron isotopes (Anagnostou et al., 2016) and would require extremely large masses of carbon to have been injected into—and subsequently removed from—the Earth system on geologically short timescales with no discernible influence on carbonate  $\delta^{13}C$  values. Here, we revisit this issue using the boron isotope ( $\delta^{11}B$ ) pH proxy (see, e.g., Foster & Rae, 2016; Hemming & Hanson, 1992) to

generate new, independent estimates of ocean pH and pCO<sub>2</sub> change at this time. We then explore the significance of our record in constraining causal mechanisms, global weathering feedbacks, and climate sensitivity over this enigmatic event.

## 2. Materials and Methods

### 2.1. Site and Species Selection

We analyzed single-species mixed-layer foraminifera primarily at the equatorial Pacific ODP Site 865 (1,300–1,500 m paleo-depth; Bralower et al., 1995), which has been the subject of previous boron isotope investigations (Edgar et al., 2015; Pearson & Palmer, 1999, 2000). To ascertain to what extent our resultant pCO<sub>2</sub> record was globally representative, we compared these data with lower-resolution measurements from three other deep-sea drill sites, spanning a wide range of oceanographic settings (Figure 2): ODP Sites 1260 (equatorial Atlantic; ~2,500–3,200 m paleo-depth; Sexton et al., 2006; Shipboard Scientific Party, 2004a), 1263 (midlatitude South Atlantic; ~2,000 m paleo-depth; Shipboard Scientific Party, 2004b), and 702 (Southern Ocean; ~2,250 m paleo-depth; Katz & Miller, 1991; Shipboard Scientific Party, 1988). High-resolution bulk carbonate or benthic foraminiferal  $\delta^{13}\text{C}$  and  $\delta^{18}\text{O}$  stratigraphies are available for each site (Bohaty et al., 2009; Boscolo Galazzo et al., 2014; Edgar et al. (subm.); Edgar et al., 2010; Sexton et al., 2006b), allowing cross-correlation. All sites are open-ocean in setting and remain above the local CCD across the event, although at ODP Site 1260 multiple clay layers are evident within the MECO (Edgar et al., 2010), indicating that this site was close to the local lysocline. It is likely, therefore, that our sampling at ODP Site 1260 misses the peak of the MECO event. Calcareous nannofossil and foraminiferal communities from ODP Site 865 indicate that sediments were deposited under oligotrophic open-ocean conditions (Bralower et al., 1995), suggesting that [CO<sub>2</sub>]<sub>aq</sub> reconstructed at these sites was likely in (near) equilibrium with the atmosphere with respect to CO<sub>2</sub>. Abundant siliceous microfossils suggest more productive surface ocean conditions at ODP Sites 1260 and 702, while productivity at ODP Site 1263 appears to vary temporally over the event (Boscolo Galazzo et al., 2015).

At each site, monospecific separates (136–343 tests, 1.8–4.3 mg CaCO<sub>3</sub>) of planktic foraminifera were picked for  $\delta^{11}\text{B}$  analyses from the 250–300  $\mu\text{m}$  sieve size range to minimize any ontogenetic or metabolic effects. We selected the shallowest-dwelling foraminiferal species possible at each site, given the sample size requirements for analysis. Specifically, these were *Globigerinatheka index* (at ODP Site 702); *Acarinina praetopilensis* (ODP Site 865); *Morozovelloides crassatus* (ODP Site 1260); and *Globigerinatheka kugleri* (ODP Site 1263). Foraminifera at all sites are recrystallized, but the degree of diagenetic recrystallization varies between sites (see Sr/Ca data, supporting information). The most pervasive alteration is seen at ODP Site 865, but even extensive recrystallization in Eocene sediments from this site appears to have had little influence on fossil foraminiferal  $\delta^{11}\text{B}$  values (Edgar et al., 2015).

### 2.2. Age Models

All ages are reported on the Geological Timescale 2012 (Gradstein et al., 2012). Sites were aligned using a combination of stable isotopic, magneto-stratigraphic, and biostratigraphic tie points. An internally consistent age model for all sites was constructed based on ODP Site 702, which has the most complete magnetostratigraphy (Clement & Hailwood, 1991) and most highly resolved bulk stable isotope stratigraphy in this study (Bohaty et al., 2009). All stable isotope tie points were calibrated at this site based on linear interpolation between magnetochron boundaries. Although magnetostratigraphy at all sites was developed with biostratigraphic controls in mind, we used bioevent tie points for age control only outside of the focal interval, at depths where no stable isotope stratigraphy or reliable magnetic data were available for correlation. This is because bioevents are difficult to employ for correlation across such a large latitudinal range used in this study, given likely faunal differences between sites at any one time. Immediately surrounding and within the MECO itself, stable isotope tie points were most useful for correlation. Our age models therefore represent a compromise between number of robust (easy-to-pick) tie points and alignment of major stable isotope features at all sites. A full list of the stable isotope tie points used in this study and the age assigned to each are shown in Table S1 and are plotted in the depth domain in Figure S1.

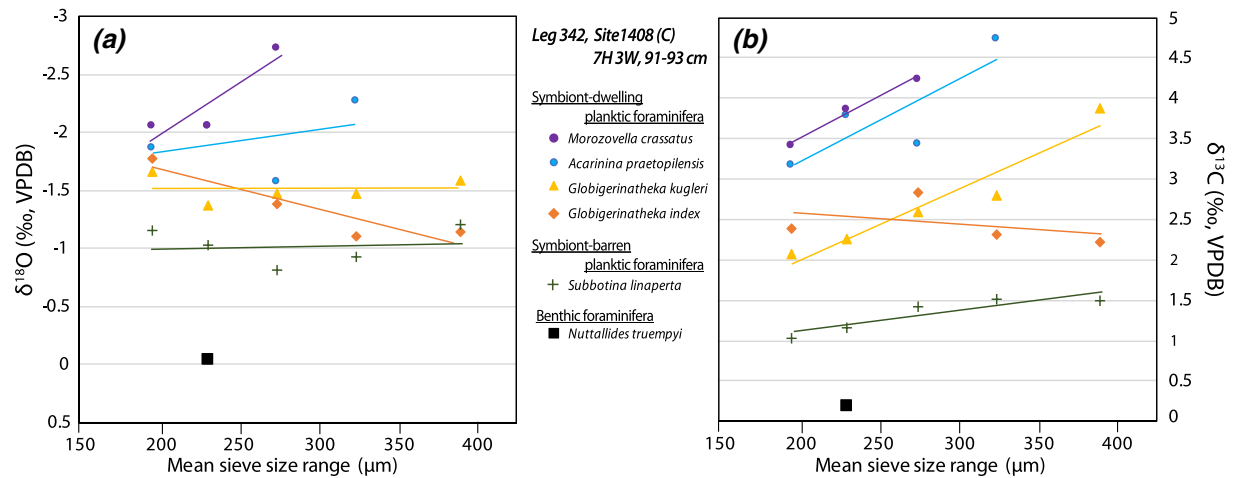


**Figure 3.** Planktic foraminiferal stable oxygen (a) and carbon (b) isotope gradients with test size for species used in this study, measured at IODP Site 1408. Preliminary age assigned to this time-slice is between 40.0 and 40.5 Ma or planktic foraminiferal Zone E12. Thermocline dwelling, symbiont-barren species *Subbotina linaperta* and benthic foraminifera *Nuttallides truempyi* are shown for comparison.

### 2.3. Analytical Methods

Boron isotope analyses were carried out on a Thermo Neptune Multi-Collector ICP-MS at the University of Southampton following Foster (2008). External reproducibility is estimated from  $^{11}\text{B}$  signal intensity (primarily dictated by sample size) using a relationship between intensity and long-term reproducibility at the University of Southampton from Greenop et al. (2017). Sample cleaning and preparation follow established protocols (see Anagnostou et al., 2016; Henehan et al., 2016, and references therein). For each sample, a subsample of cleaned, crushed foraminiferal carbonate was taken for  $\delta^{13}\text{C}$  and  $\delta^{18}\text{O}$  analyses, while an aliquot of dissolved material was taken prior to boron column chemistry for trace and minor element analysis (B, Mg, Al, and Sr). Trace element analysis was carried out using a Thermo Element ICP-MS at the University of Southampton. Long-term reproducibility (2 SD) was  $\pm <5\%$  for Al/Ca ratios measurements, and  $\pm <3\%$  for Mg/Ca and Sr/Ca. Al/Ca ratios for samples analyzed here are all  $<105 \mu\text{mol/mol}$ , below an operational threshold of  $\sim 140 \mu\text{mol/mol}$  commonly used to indicate clay contamination (Rae et al., 2011). Foraminiferal  $\delta^{13}\text{C}$  and  $\delta^{18}\text{O}$  analyses from ODP Sites 702, 865, 1260, and 1263 were made on a Thermo Scientific Delta V Advantage mass spectrometer coupled to a GasBench II at Cardiff University and are reported relative to the Vienna Pee Dee Belemnite (VPDB) standard with an external analytical precision ( $1\sigma$ ) of  $0.06\text{‰}$  for  $\delta^{13}\text{C}$  and  $0.07\text{‰}$  for  $\delta^{18}\text{O}$ . Further samples from IODP Site U1408 were measured for  $\delta^{13}\text{C}$  and  $\delta^{18}\text{O}$  on a Thermo Kiel IV coupled to a Thermo MAT 253 mass spectrometer at Yale University, with typical external precision ( $1\sigma$ ) of  $<0.03\text{‰}$  for  $\delta^{13}\text{C}$  and  $<0.04\text{‰}$  for  $\delta^{18}\text{O}$  based on replicate analyses of in-house (TS, MERC, CM, and PX) and international (NBS19) standards.

### 2.4. Vital Effects

To calculate ocean pH from foraminiferal  $\delta^{11}\text{B}$  values, one must first consider the possible influence of “vital effects.” Photosynthetic activity of symbiotic algae elevates seawater pH in the immediate microenvironment around host planktic foraminifera, while symbiont and host respiration lowers pH (see, e.g., Henehan, Foster, et al., 2016; Hönisch et al., 2003; Jørgensen et al., 1985; Köhler-Rink & Köhl, 2005; Zeebe et al., 2003). Because of varying rates of photosynthesis and respiration, foraminiferal species living in similar ambient seawater pH may record different  $\delta^{11}\text{B}$  values (see, e.g., Anagnostou et al., 2016; Henehan, Foster, et al., 2016; Hönisch et al., 2003). While almost all studied modern planktic foraminifera record  $\delta^{11}\text{B}$  values offset from ambient  $\delta^{11}\text{B}_{\text{borate}}$  (Anagnostou et al., 2016; Henehan, Foster, et al., 2016, and references therein), recent work has suggested that vital effects were dampened in the Eocene relative to today (Anagnostou et al., 2016), and as such, further investigation was necessary.

Vital effects in extinct species can be gauged by comparison of  $\delta^{11}\text{B}$ ,  $\delta^{13}\text{C}$ ,  $\delta^{18}\text{O}$ , and B/Ca ratios across a foraminiferal assemblage (Anagnostou et al., 2016; Edgar et al., 2015; Henehan, Foster, et al., 2016) and/or

using intra-specific body size  $\delta^{13}\text{C}$  and  $\delta^{18}\text{O}$  gradients (Birch et al., 2012; D'Hondt et al., 1994; Edgar et al., 2013; Ezard et al., 2015; Pearson et al., 1993; Sexton, Wilson, & Pearson, 2006b). To constrain vital effects in the species measured here, we made new  $\delta^{13}\text{C}$  and  $\delta^{18}\text{O}$  measurements of well-preserved “glassy” foraminifera from IODP Site U1408 where all of the species measured here coexisted in a single time-slice (Norris et al., 2014) (Figure 3). This new  $\delta^{13}\text{C}$  and  $\delta^{18}\text{O}$  data support a shallow mixed-layer habitat for *A. praetopilensis* and *M. crassatus*. However, our data support a somewhat deeper mixed-layer habitat for *G. index* and *G. kugleri*, as suggested elsewhere (Anagnostou et al., 2016; Edgar et al., 2013, 2015; Pearson et al., 1993, 2001, 2006; Sexton, Wilson, & Pearson, 2006b). Globigerinathekids record cooler  $\delta^{18}\text{O}$  temperatures than *M. crassatus* and *A. praetopilensis* (Figure 3a), with *G. index* in particular indicating progressively deeper habitat in size fractions larger than those analyzed here, perhaps reflecting the addition of gametogenic crusts at depth (Pearson et al., 1993; Premoli Silva et al., 2006; Sexton, Wilson, & Pearson, 2006b). With regards  $\delta^{13}\text{C}$ , globigerinathekids at Site U1408 record lower values than *M. crassatus* or *A. praetopilensis*, indicating weaker photosynthetic activity in their microenvironment and/or a deeper mean habitat. While *G. kugleri* displays a strong positive  $\delta^{13}\text{C}$  gradient with increasing size (Figure 3b) consistent with symbiont-bearing foraminifera (Ezard et al., 2015; Pearson et al., 1993; Spero et al., 1991), *G. index* does not, suggesting that high latitude *G. index* had few or no photosynthetic symbionts. Thus, our focal species likely have varying degrees of influence from photosymbionts. By analogy with extant taxa, these species are expected to display variable offsets from aqueous  $\delta^{11}\text{B}_{\text{borate}}$  (Henehan, Foster, et al., 2016). We therefore assign calibrations by analogy with modern taxa based on our  $\delta^{13}\text{C}$  and  $\delta^{18}\text{O}$  data and published observations (Anagnostou et al., 2016; Edgar et al., 2013; Pearson et al., 1993, 2001; Sexton, Wilson, & Pearson, 2006b). For *A. praetopilensis* and *M. crassatus*, we apply a calibration based on the low-latitude, mixed-layer dwelling, dinoflagellate-bearing *Trilobatus sacculifer* (Foster et al., 2012). For deeper mixed-layer *G. kugleri*, we apply a calibration based on the similarly deeper-dwelling symbiont-bearing species *Orbulina universa* (Henehan, Foster, et al., 2016). For *G. index*, which lacks any gradient in  $\delta^{13}\text{C}$  with size (Figure 3b), we apply the symbiont-barren calibration for *Globigerina bulloides* (Martínez-Botí et al., 2015). In each case, calibration lines were adjusted to account for a middle Eocene seawater  $\delta^{11}\text{B}$  ( $\delta^{11}\text{B}_{\text{sw}}$ ) of 38.7‰ using the approach of Greenop et al. (2019). This is necessary, as otherwise modern calibrations conflate the effects of pH and  $\delta^{11}\text{B}_{\text{sw}}$  on deep time records (see Greenop et al., 2019, for more details).

We note also that reduced body size  $\delta^{13}\text{C}$  gradients in *Acarinina* during peak MECO at ODP Sites 1051 and 748 have been interpreted as symbiont “bleaching” (Edgar et al., 2013; see also Wade et al., 2008). Since this could modify the pH of the foraminiferal microenvironment and artificially produce or accentuate a surface ocean pH drop, we tested whether bleaching occurred at the MECO by examining body size  $\delta^{13}\text{C}$  gradients at tropical ODP Sites 865 and 1260, where temperature-driven “bleaching” might be most evident. However, we found no evidence for a reduction in either the  $\delta^{13}\text{C}$  gradient between symbiont-bearing and symbiont-barren taxa or the body size  $\delta^{13}\text{C}$  gradient in the species analyzed here (Figure S2). This suggests that a loss of symbionts did not occur at these low-latitude sites and that any  $\delta^{11}\text{B}$  changes should therefore reflect changes in ambient seawater pH rather than changing vital effects.

### 2.5. pH and Temperature Calculations and Uncertainty Propagation

To calculate pH accurately from  $\delta^{11}\text{B}$ , a number of auxiliary parameters are required, including  $\delta^{11}\text{B}_{\text{sw}}$ , salinity, and temperature. Using the approaches of Anagnostou et al. (2016) (viz., assuming reasonable bounds on surface ocean saturation and vertical DIC gradients) and a  $\delta^{11}\text{B}_{\text{sw}}$ -corrected *T. sacculifer* calibration for their mixed-layer dwelling, symbiont-bearing early and middle Eocene foraminifera, we calculate absolute bounds of  $\delta^{11}\text{B}_{\text{sw}}$  of 38.5–38.9‰ at this time. We assign a salinity of  $34 \pm 1$  psu to all samples (note that this parameter has only a small effect on pH and  $\text{pCO}_2$  estimates; e.g., Henehan et al., 2013). To estimate sea surface temperature, we used planktic foraminiferal Mg/Ca ratios, as they appear more robust in the face of diagenetic recrystallization than  $\delta^{18}\text{O}$  (Sexton et al., 2006a). However, modern Mg/Ca temperature calibrations cannot be directly applied to middle Eocene foraminifera, because of the different  $\text{Mg}/\text{Ca}_{\text{sw}}$  at this time and the (sizeable) effect of pH on foraminiferal Mg/Ca (e.g., Evans et al., 2016; Gray & Evans, 2019). All our temperature calculations are therefore corrected for the nonlinear response of foraminiferal Mg/Ca to changing  $\text{Mg}/\text{Ca}_{\text{sw}}$  following Evans et al. (2016). Since pH calculations require temperature estimates, and vice versa, we iteratively correct both parameters, similar to methods given by Gray and Evans (2019).

Low Eocene seawater pH means that pH corrections on Mg/Ca-derived temperatures are sizeable (Figure S3). To our knowledge, these are the first Mg/Ca<sub>sw</sub> and pH-corrected temperatures for this period and thus provide new constraints on sea surface temperatures across a latitudinal gradient in the middle Eocene.

For uncertainty propagation, we used Monte Carlo simulations in R (R Core Team, 2015). For pH estimates, 500  $\delta^{11}\text{B}_{\text{calcite}}$  values were randomly generated from within a normal distribution described by  $2\sigma$  analytical reproducibility for each data point (see Table S1). Each value was then converted to  $\delta^{11}\text{B}_{\text{borate}}$  according to each species'  $\delta^{11}\text{B}_{\text{sw}}$ -specific calibration (see section 2.4). Major ion chemistry-specific equilibrium constants (from Hain et al., 2015) for each value were calculated according to preliminary Mg/Ca-derived temperatures (from 500 simulations of Mg/Ca within 3% analytical uncertainty, corrected for Mg/Ca<sub>sw</sub>; Evans, Brierley, et al., 2016), but not pH (Evans, Wade, et al., 2016), and 500 randomly generated values of salinity (within  $34 \pm 1$ ). pH was then calculated for each simulated value and used to derive the “excess Mg/Ca” due to low pH (according to the linear fit of Evans, Wade, et al., 2016). pH-corrected temperatures were then calculated for each Monte Carlo replicate and subsequently used to recalculate equilibrium constants and pH. This was iterated until simulated replicates converged on a unique solution to within 0.002 pH. Final temperature and pH estimates were calculated as the mean of the 500 Monte Carlo simulations, with 95% interquartile range of these replicates taken as uncertainty. In these calculations, we include uniformly distributed uncertainty on  $\delta^{11}\text{B}_{\text{sw}}$  within the range of 38.5–38.9‰ (Anagnostou et al., 2016), when presenting true uncertainty on absolute values of pH. However, the long residence time of boron in the ocean (~10 to 20 Myr) means that  $\delta^{11}\text{B}_{\text{sw}}$  would have remained constant across the time interval studied here, and so uncertainty on relative changes in pH is considerably smaller. To isolate the effect of  $\delta^{11}\text{B}_{\text{sw}}$  on relative pH changes and provide the basis for LOSCAR simulations discussed later in section 2.7, we also calculated pH across a range of discrete values of  $\delta^{11}\text{B}_{\text{sw}}$ . We do not attempt to propagate uncertainty in Eocene major ion chemistry or (small) salinity effects on foraminiferal Mg/Ca (Hönisch et al., 2013) since quantitative constraints over this interval are limited.

## 2.6. pCO<sub>2</sub> Calculations

To calculate pCO<sub>2</sub> from surface ocean pH, one requires one other carbonate system parameter (Zeebe & Wolf-Gladrow, 2001). Because we have no suitable proxy record to obtain this second parameter, we explore a number of possible scenarios using simplified assumptions to represent end-member pCO<sub>2</sub> possibilities. First, we calculate pCO<sub>2</sub> assuming a constant calcite saturation state ( $\Omega_{\text{calcite}}$ ) in the surface ocean at each site. This assumption represents a scenario in which alkalinity increases driven by elevated silicate weathering and carbonate dissolution could effectively keep pace with the pH decline calculated from  $\delta^{11}\text{B}$ . Specifically, in our Monte Carlo simulations, we allow starting  $\Omega_{\text{calcite}}$  to vary within a uniform distribution between 5.75 and 7.5 at Sites 865 and 1260; 5.25 and 7.25 at Site 1263; and 3.75 and 5.25 at Site 702, with differences reflecting each site's paleolatitude (following Anagnostou et al., 2016). For each Monte Carlo simulation,  $\Omega_{\text{calcite}}$  was then held constant through the MECO, and the carbonate system solved to calculate pCO<sub>2</sub>, according to the carbonate equilibrium constants and calcite solubility product calculated for each data point.

As a second end-member scenario, we performed pCO<sub>2</sub> calculations using the assumption that surface ocean total alkalinity (TALK) remained constant throughout the event. By contrast with the constant  $\Omega_{\text{calcite}}$  scenario, this assumption implies that silicate weathering and carbonate compensation were too weak to significantly affect surface ocean carbonate chemistry during the MECO and that changes in pH reflect the addition of DIC alone. This assumption of constant TALK would be more consistent with a postulated weakened silicate weathering feedback strength across the MECO (van der Ploeg et al., 2018). To obtain a pre-event surface ocean TALK estimate, we took pre-event equilibrium values from simulations of the geochemical box model LOSCAR, matched to pre-event mean LOESS pH fit (see section 2.7). We then held this alkalinity constant at within  $\pm 150 \mu\text{Mol}$  of LOSCAR's pre-MECO surface ocean TALK estimate throughout the MECO.

## 2.7. Carbon Cycle Modeling MECO Acidification

Regrettably, the complex, spatially variable and as-yet poorly constrained array of potential influences on carbonate  $\delta^{13}\text{C}$  values during the MECO mean that reverse modeling the event (e.g., as done for the

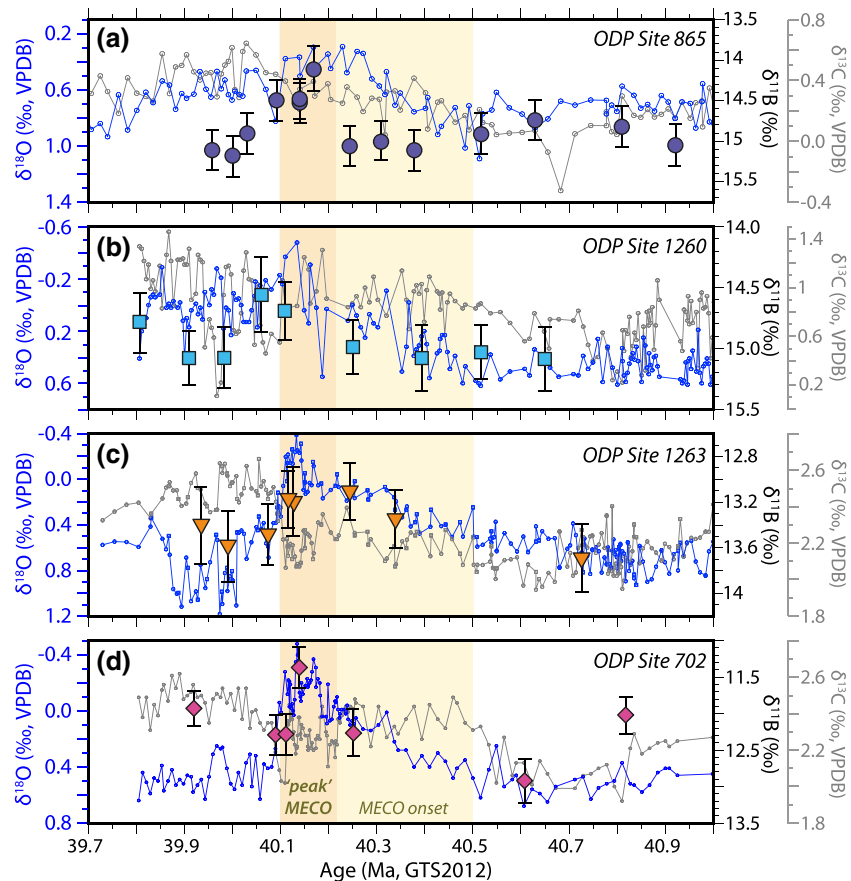


**Figure 4.** Measured planktic foraminiferal  $\delta^{11}\text{B}$  at each site in the context of local  $\delta^{13}\text{C}$  and  $\delta^{18}\text{O}$  data. These data are as follows: (a) benthic foraminiferal  $\delta^{13}\text{C}$  and  $\delta^{18}\text{O}$  data from ODP Site 865 (Edgar et al., *subm.*); (b) benthic foraminiferal  $\delta^{13}\text{C}$  and  $\delta^{18}\text{O}$  data from ODP Site 1260 (Edgar et al., 2010; Sexton, Wilson, & Norris, 2006); (c) bulk sediment  $\delta^{13}\text{C}$  and  $\delta^{18}\text{O}$  data from ODP Site 1263 (Bohaty et al., 2009) and (d) bulk sediment  $\delta^{13}\text{C}$  and  $\delta^{18}\text{O}$  data from ODP Site 702 (Bohaty et al., 2009).  $\delta^{18}\text{O}$  data are shown in blue,  $\delta^{13}\text{C}$  data are in gray, and  $\delta^{11}\text{B}$  data are colored according to their site marker in Figure 1. Error bars on  $\delta^{11}\text{B}$  data represent  $2\sigma$  uncertainty estimated from  $^{11}\text{B}$  signal intensity based on long-term replicates of JCP-1 Porites coral standard (Okai et al., 2002) (see section 2).

PETM by Gutjahr et al., 2017) is not yet feasible. However, because LOSCAR (Long-term Ocean Sediment Carbon Reservoir, v2.0.4; Zeebe, 2012) approximates some critical processes for interpreting pH records—namely, the changes in chemical weathering and carbonate burial one would normally associate with  $\text{pCO}_2$  rise—we could use it to further explore feasible changes in  $\text{pCO}_2$  over the MECO across a broad range of possible  $\delta^{11}\text{B}_{\text{sw}}$ . More specifically, we leveraged LOSCAR to obtain estimates for  $\text{pCO}_2$  from MECO carbon cycle model scenarios that were constrained only by  $\delta^{11}\text{B}$ -derived pH. To do this, we used LOSCAR’s “PALEO” configuration (with a Tethys ocean and Paleogene circulation patterns and bathymetry) but with some modifications. First, we replaced the default corrections for [Mg] and [Ca] (Ben-Yaakov & Goldhaber, 1973) with updated equilibrium constants that better quantify ion pairing effects (Hain et al., 2015) by accounting for the activities of all ions in solution using the larger and more up-to-date MIAMI database (Millero & Pierrot, 1998), using a seawater [Mg] and [Ca] of 38 and 17 mM, respectively. Second, to more finely resolve deep water carbonate dissolution and compensation depth, we modeled one sediment level every 100 m, rather than the default 500 m (following Henehan, Hull, et al., 2016).

To obtain pre-MECO alkalinity estimates for any given  $\delta^{11}\text{B}_{\text{sw}}$  scenario, the model was equilibrated by adjusting equilibrium  $\text{pCO}_2$  in 10 Myr-long spin-up runs with a default strength silicate weathering feedback ( $N_{\text{Si}} = 0.2$ ) until we attained a fit between LOSCAR’s low-latitude surface Pacific box and boron-derived

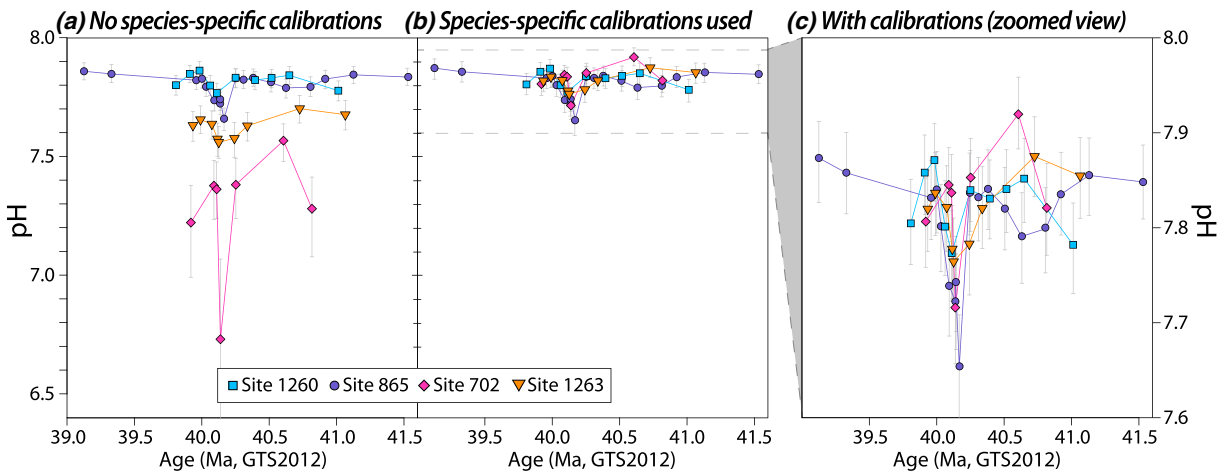


**Figure 5.** Boron-derived pH reconstructions from the four study sites without vital effect calibrations (a) and applying species-specific calibrations (b). Note that these calculations assume  $\delta^{11}\text{B}_{\text{sw}}$  of 38.5–38.9‰,  $[\text{Mg}]_{\text{sw}} = 38 \text{ mM}$ , and  $[\text{Ca}]_{\text{sw}} = 17 \text{ mM}$  and temperature estimates from planktic foraminiferal Mg/Ca (see section 2.5).

pre-MECO surface ocean pH values (to within 0.002 pH units). This target pH for a given  $\delta^{11}\text{B}_{\text{sw}}$  was calculated as the mean of the first 17 values of the mean LOESS fit prior to the pH drop at the peak MECO. For each value of  $\delta^{11}\text{B}_{\text{sw}}$ /starting pH, we then iteratively added different masses of  $\text{CO}_2$  to the atmosphere over the timescale of our peak MECO pH excursion (~100 kyr) until we produced a surface Pacific pH decrease that matched the minimum value in the  $\delta^{11}\text{B}$ -derived LOESS pH curve to within 0.002 pH units. This exercise was repeated across a broad range of  $\delta^{11}\text{B}_{\text{sw}}$  (37.4–39.5‰), and in each case,  $\Delta\text{pCO}_2$  was calculated as the difference in  $\text{pCO}_2$  from spin-up to peak MECO.  $\text{CO}_2$  forcing change ( $\Delta F$ ) was then calculated from  $\Delta\text{pCO}_2$ , according to the relationship of Myhre et al. (1998). Our primary simulations used default parameterized climate sensitivity in LOSCAR of 3 °C warming per doubling of atmospheric  $\text{pCO}_2$ . Since calculated warming influences  $\text{CO}_2$  solubility, DIC speciation, and carbonate solubility calculations in LOSCAR, we also repeated our experiments with a prescribed 2 °C warming over the 100 kyr carbon release event to test for the influence of this parameter, with negligible effect on our  $\text{CO}_2$  estimates (at  $\delta^{11}\text{B}_{\text{sw}} = 38.7\text{‰}$ ,  $\Delta\text{pCO}_2$  changes by <0.002 doublings).

### 3. Results

#### 3.1. Boron Isotope Records

Boron isotope measurements are shown in Figure 4. The main feature of our record at our main site, ODP Site 865, is a transient ~1‰  $\delta^{11}\text{B}$  decrease focused around minimum MECO  $\delta^{18}\text{O}$  values (~40.22–40.10 Ma, hereafter “peak MECO”), followed by return to pre-event values (Figure 4). Despite some discrepancies (Figures 4b–4d), our lower-resolution sites generally corroborate the observed trends at Site 865 well, especially when considering the stratigraphic challenges of correlating each record (see, e.g., Figure S1). With no further assumptions, this drop in  $\delta^{11}\text{B}$  values constitutes the first empirical evidence for surface ocean acidification over the MECO and at face value supports a rise of atmospheric  $\text{pCO}_2$  associated with the event. Notably, though, the  $\delta^{11}\text{B}$  excursion at peak MECO where our samples are best resolved is brief (~120 kyr from onset to recovery), with limited, if any, change during the preceding ~280 kyr of global  $\delta^{18}\text{O}$  decline (~40.5–40.22 Ma, hereafter “MECO onset”).

#### 3.2. Calculated pH Change at the MECO

To examine whether our choices of vital effect calibrations are reasonable, we compare pH calculated from  $\delta^{11}\text{B}$  with and without consideration of vital effects in Figure 5. We observe very large latitudinal offsets in  $\delta^{11}\text{B}$  values (~3.3‰; Figure 4). Without applying calibrations for vital effects at the MECO, even accounting for temperature (and hence  $\text{pK}^*_\text{B}$ ) variations with latitude, gives a latitudinal pH gradient of up to 1.2 (Figure 5a), that cannot reasonably be explained even considering a possibly deeper depth habitat for

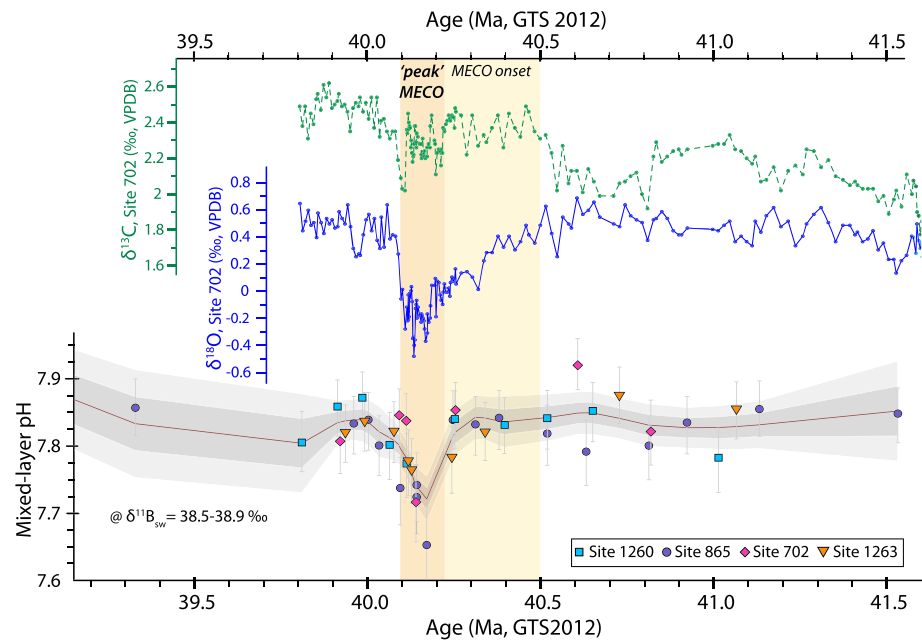


**Figure 6.** Mean global surface ocean pH and  $p\text{CO}_2$  change from boron isotopes. All sites are stacked to create a global loess-smoothed pH curve, shown in context of  $\delta^{13}\text{C}$  and  $\delta^{18}\text{O}$  values from bulk carbonate at ODP Site 702 (Bohaty et al., 2009) (the site to which other sites' age models are tied). Dark and light gray shaded areas represent 95% and 68% confidence intervals, respectively, as determined by 500 Monte Carlo simulations of LOESS fits on simulated data sets within the propagated uncertainty of each pH data point. Calculations here are for a  $\delta^{11}\text{B}_{\text{sw}}$  of 38.5–38.9‰.

*G. index*. Such a large pH offset would translate to considerable  $[\text{CO}_2]_{\text{aq}}$  variation between sites and  $\text{CO}_2$  disequilibrium between ocean and atmosphere of  $>4,500 \mu\text{atm CO}_2$  at Site 702 (for alkalinity  $>1,000 \mu\text{mol/kg}$ ), which is not plausible. Besides this, at the pH values inferred at Site 702, for an ocean alkalinity ranging from 1,000–3,000  $\mu\text{mol/kg}$ ,  $\Omega_{\text{calcite}}$  would reach as low as 0.2–0.4 at peak MECO. This would require *G. index* and other calcifiers at Site 702 to have persisted in waters highly undersaturated with respect to calcite, with few if any analogues for such behavior today. In contrast, our pH estimates agree closely once vital effects are accounted for as described above (Figure 5b), suggesting our assignment of calibrations from modern analogue species according to  $\delta^{13}\text{C}$  and  $\delta^{18}\text{O}$  is reasonable. These data therefore indicate that vital effects in foraminiferal  $\delta^{11}\text{B}$  were present at least in middle Eocene globigerinathekids and thus may well have been present in other extinct species too. We note, however, that the magnitude of vital effects in *A. praetopilensis* and *M. crassatus* predicted by the Foster et al. (2012) *T. sacculifer* calibration is very small, and so the agreement between calibrated globigerinathekids and uncalibrated *A. praetopilensis* and *M. crassatus* is not significantly worse than when modern analogue calibrations are applied to all species (see Figure S4). Further research, considering among other things changes in  $\delta^{11}\text{B}$  with size fraction (see, e.g., Henahan, Foster, et al., 2016), is therefore required to determine whether modern analogue calibrations must be applied to *Morozovella* and *Acarinina* species.

As with any geological observation, corroboration of a signal at multiple sites globally allows more confidence in results. Additionally, multisite analyses allow us to test the feasibility of vital effect corrections in the Eocene (Figure 5), reducing an otherwise large structural uncertainty in our pH and  $p\text{CO}_2$  estimates. However, combining data from four geographically disparate sites as we do here does present complications, with the obvious introduction of aliasing (Pisias & Mix, 1988) from our low-resolution sites (e.g., ODP Site 1260, where the peak MECO is not sampled), noise from uncertainty in stratigraphic correlation (e.g., see Figure S1), and possible regional hydrographic differences (e.g., variable productivity, and hence perhaps air-sea disequilibrium, at ODP Site 1263 over the MECO; Boscolo Galazzo et al., 2015). In all likelihood, all of these processes are at work within our records. The intersite pH variability, taken at face value, at

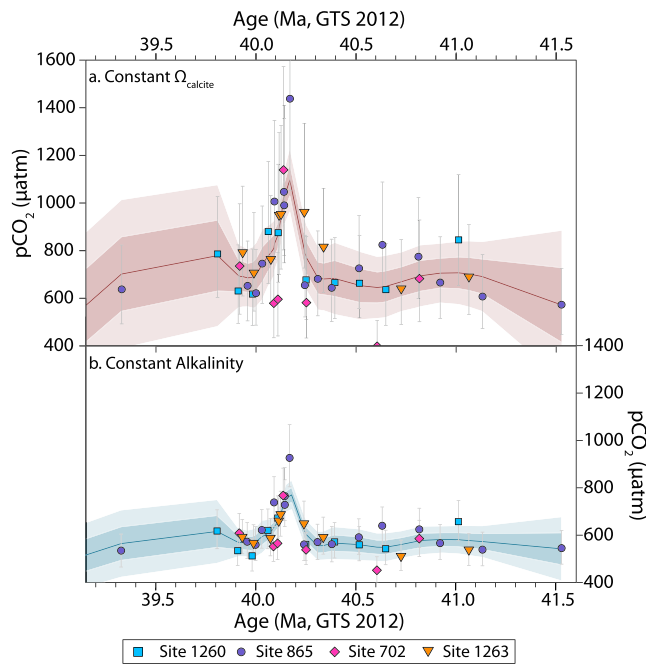


**Figure 7.** pCO<sub>2</sub> across the MECO calculated assuming either constant surface ocean saturation state (a) or constant surface ocean alkalinity (b), for our best estimate of  $\delta^{11}\text{B}_{\text{sw}}$  (38.5–38.9‰).

any given time within our record (Figure 5) is sometimes larger than could easily be simulated with earth system models, suggesting that inaccuracy in stratigraphic correlation likely plays a role in adding noise to our record. Consequently, so as not to risk overinterpreting scatter from these various sources of error at any one site and to facilitate modeling work, we calculate a smoothed, globally averaged surface ocean  $\Delta\text{pH}$  LOESS curve for the MECO (Figure 6).

To calculate the LOESS curve, we combined all sites'  $\delta^{11}\text{B}$ -pH measurements using a best-fit LOESS where the degree of smoothing was optimized using a generalized cross-validation algorithm (Golub et al., 1979) which objectively gauges the most statistically supported value for the LOESS span (using code from M. Friendly, <http://www.datavis.ca>). Because the rates of pH change are important, we incorporated some uncertainty in the age domain, based on the sedimentation rate estimates between tie points, along with uncertainty in calculated pH. Specifically, 500 independent LOESS lines were fitted to each of the 500 replicate Monte Carlo pH data sets outlined above, with 500 simulated ages for each data point generated from within the age range of the sampling interval. For a  $\delta^{11}\text{B}_{\text{sw}}$  of 38.5–38.9‰, our data indicate a pH decrease of  $0.12 \pm 0.04$  over <100 kyr coincident with the peak MECO (Figure 6). The objective smoothing algorithm used in our global LOESS fit does however dampen the transient reduction of up to  $\sim 0.18$  pH units implied by a single point at our most highly resolved site, ODP 865 (Figure 4), and so it is possible that further higher resolution studies may find our estimates of pH change to be conservative.

A somewhat surprising aspect of our LOESS global mean pH record is the lack of a pronounced decline in mean ocean pH during the onset phase of the MECO, when global temperature records suggest gradual warming (e.g., Bohaty et al., 2009). There are some apparent discrepancies between sample sites during this interval: At ODP Site 1263,  $\delta^{11}\text{B}$  drops more in line with global  $\delta^{18}\text{O}$  decline than observed at Sites 865 or 1260. However, since higher resolution sites show no such rise, and statistically none of the four sites show a significant trend in pH before the peak of the MECO (Figure S5), we avoid overinterpreting intersite differences here.

### 3.3. pCO<sub>2</sub> Change Over the MECO

pCO<sub>2</sub> calculated from surface ocean pH is shown for a constant saturation state (Figure 7a) and a constant LOSCAR-derived TALK of  $1,750 \pm 150$  μmol/kg (Figure 7b). In the case of a constant  $\Omega$ , pre-MECO pCO<sub>2</sub> (as defined in this instance as the mean of the LOESS values during the earliest 17 pre-MECO data points) is  $\sim 669 \pm 145$  μatm, with the maximum of the pCO<sub>2</sub> LOESS rising to  $\sim 1,062 \pm 127$  μatm at the peak MECO (equating to  $0.67^{+0.17}_{-0.12}$  doublings). Assuming a constant ( $\pm 150$  μmol/kg) alkalinity instead, our boron isotope data would suggest a pCO<sub>2</sub> rise from  $\sim 563 \pm 67$  μatm to  $\sim 770 \pm 62$  μatm at the peak MECO, a rise that is  $\sim 47\%$  smaller than if calcite saturation remained constant. As these two end-member scenarios represent extreme limits to the possible real-world response, we suggest that the pCO<sub>2</sub> increase during the MECO was likely somewhere between these two scenarios.

From our LOSCAR simulations (Figure 8), it may be seen that while absolute values of pCO<sub>2</sub> calculated are sensitive to  $\delta^{11}\text{B}_{\text{sw}}$  (Figure 8b), relative change in greenhouse forcing in terms of CO<sub>2</sub> doublings is relatively insensitive to changes in this parameter (i.e., 0.55 to 0.75 CO<sub>2</sub> doublings for  $\delta^{11}\text{B}_{\text{sw}}$  between 37.5‰ and 39.5‰; Figure 8c). This has been similarly demonstrated at the Eocene-Oligocene transition (Pearson et al., 2009) and at the PETM (Penman & Zachos, 2018). Using our LOSCAR modeling approach, instead of assuming constant  $\Omega_{\text{calcite}}$  or alkalinity, our best-estimate middle Eocene  $\delta^{11}\text{B}_{\text{sw}}$  range of 38.5–38.9‰ produces  $\Delta\text{pCO}_2$  scenarios from pre-MECO (i.e., background) to the peak MECO of 500 μatm rising to 765 μatm for a  $\delta^{11}\text{B}_{\text{sw}}$  of 38.5‰ and 630 μatm rising to 990 μatm for a  $\delta^{11}\text{B}_{\text{sw}}$  of 38.9‰ (Figure 8b). Expressed as doublings of CO<sub>2</sub>, these end-member scenarios for  $\Delta\text{pCO}_2$  equate to between 0.62 and 0.67, which translates to a

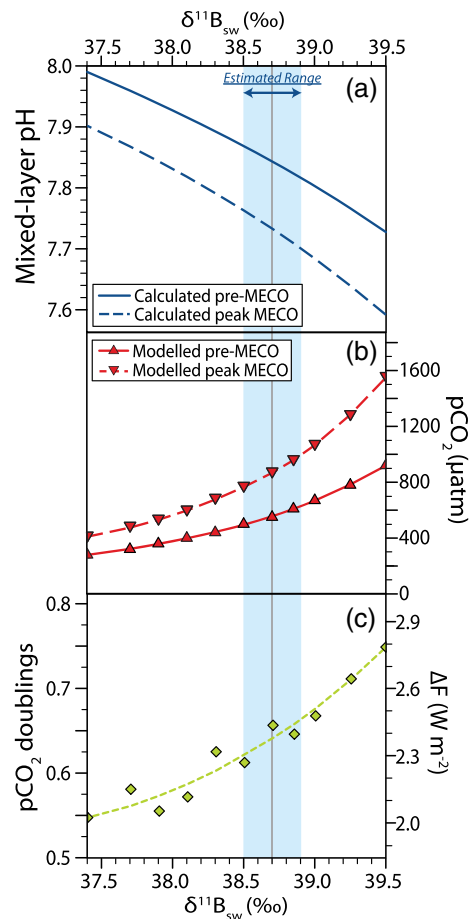


**Figure 8.** For each given value of  $\delta^{11}\text{B}_{\text{sw}}$ , calculated “pre-event” pH values (solid blue line, the average of the pH values prior to the peak MECO excursion), and the minimum value reached by the global LOESS during peak MECO (dashed blue line) are shown in panel a. In panel b, the atmospheric  $\text{pCO}_2$  required for LOSCAR to attain “pre-event” pH values (solid red line and triangles) is shown. We then iteratively simulated injection of different carbon masses over the timescales of our pH drop ( $\sim 100$  kyr) until we attained a surface Pacific pH that matched the pH minimum in our LOESS curve calculated for that  $\delta^{11}\text{B}_{\text{sw}}$  and noted the atmospheric  $\text{pCO}_2$  attained by LOSCAR (dashed red line and inverted triangles). Panel c shows the change in  $\text{pCO}_2$  in panel b, expressed in terms of  $\text{CO}_2$  doublings, and as  $\text{CO}_2$  forcing change,  $\Delta F$  (calculated according to Myhre et al., 1998). Our best estimate of  $\delta^{11}\text{B}_{\text{sw}}$  (38.5–38.9‰) is shown by the vertical blue bar through (a), (b) and (c) and implies 0.6–0.7 doublings of  $\text{pCO}_2$  over the MECO event.

$\text{CO}_2$  forcing change ( $\Delta F$ ) of between 2.3 and 2.5  $\text{W m}^{-2}$  (Figure 8c). To quantify the absolute uncertainty bounds on  $\text{pCO}_2$  within our best-estimate range of  $\delta^{11}\text{B}_{\text{sw}}$ , we repeated these LOSCAR modeling exercises for 1 and 2 SE of the 500 Monte Carlo LOESS values for pre-event pH and peak MECO pH minimum (i.e., gray shaded regions in Figure 6), to calculate a pre-event  $\text{pCO}_2$  of  $565_{-80}^{+110}$ , and a peak MECO  $\text{pCO}_2$  of  $880_{-100}^{+130}$ , as plotted in Figure S6. These pre-MECO  $\text{pCO}_2$  levels are somewhat lower in an absolute sense compared to those values calculated assuming constant, pre-ascribed  $\Omega_{\text{calcite}}$ . This is because our LOSCAR simulations produce values of  $\Omega_{\text{calcite}}$  in the surface Pacific of  $\sim 5$  throughout the MECO, which is on the lowest end of our assumed feasible Eocene range of  $\Omega_{\text{calcite}}$  and thus implies lower equilibrium TALK values at this time. However, despite this difference in absolute values, a rise of  $0.67_{-0.12}^{+0.17}$  doublings for the constant  $\Omega_{\text{calcite}}$  scenario falls squarely in the range of estimates produced by LOSCAR. By contrast, assuming constant alkalinity produces a smaller rise in  $\text{pCO}_2$  upon a similar pre-MECO baseline ( $0.45_{-0.05}^{+0.06}$ ), because without any concurrent rise in TALK, a smaller rise in DIC is required to affect the same change in pH.

## 4. Discussion

### 4.1. MECO $\text{CO}_2$ Change and Carbon Cycling

Our new boron isotope record helps to resolve some enigmatic features of the MECO. For example, an abrupt ( $< 10$  kyr) rise in atmospheric  $\text{pCO}_2$  centered around the peak of the MECO (Figure 7) could help to explain why the CCD shoaled even at the peak of a  $\sim 400$  kyr interval of apparent gradual warming—a key element of the so-called MECO “carbon cycle conundrum” (Sluijs et al., 2013). A shorter  $\text{CO}_2$  pulse could have surpassed the timescales on which chemical weathering responds to maintain oceanic  $\text{CaCO}_3$  saturation state ( $\sim 10^4$ – $10^5$  year) (Colbourn et al., 2015), thereby prompting deep-sea carbonate dissolution similar to that seen during hyperthermals (e.g., Zachos et al., 2005). The source of such a carbon injection remains enigmatic however, particularly given the lack of any global excursion toward negative  $\delta^{13}\text{C}$  at this time (Bohaty et al., 2009; Boscolo Galazzo et al., 2014; Edgar et al., 2010). Our lower estimates for background  $\text{pCO}_2$  and change in  $\text{pCO}_2$  over the MECO relative to previous reconstructions (Bijl et al., 2010) alleviate this problem somewhat, in necessitating lower masses of  $\text{CO}_2$  injection into, and removal from, the surface ocean-atmosphere system. This also helps to reconcile a rapid cooling and drawdown of  $\text{CO}_2$  after the MECO with the absence of any carbonate overshoot due to silicate weathering, such as is seen at the PETM (Penman et al., 2016). We note that enhanced burial of organic carbon, such as is observed in the Peri-Tethys of Italy (Spofforth et al., 2010) and the Crimea-Caucasus (Benyamovskiy, 2012), and consistent with globally increased  $\delta^{13}\text{C}$  in carbonates following the MECO (Bohaty et al., 2009), may have also played an important role in carbon drawdown.

Our finding that there was limited change in atmospheric  $\text{pCO}_2$  during the onset phase of the MECO, however, even while carbonate  $\delta^{18}\text{O}$  (Bohaty et al., 2009) and biomarker-based proxies (Bijl et al., 2010; Cramwinckel et al., 2018) suggest global temperatures were rising steadily over  $> 200$  kyr is a notable feature. To place a probabilistic bound on the maximum  $\text{pCO}_2$  rise permitted by our data during the onset interval, we used a Monte Carlo approach, simulating 1,000 data sets of pH across the “MECO onset” (40.5–40.21 Ma) at our preferred estimate of  $\delta^{11}\text{B}_{\text{sw}}$  by randomly sampling within the range of uncertainty of each data point. We couple these to a constant approximate pre-MECO surface ocean alkalinity estimate from LOSCAR

( $1,750 \pm 150 \mu\text{mol/kg}$ ) to calculate the trend in  $p\text{CO}_2$  predicted over the MECO onset interval. Using this approach, the mean simulated  $\Delta p\text{CO}_2$  over the MECO onset was  $+29 \mu\text{atm}$ . In the parlance of the IPCC (IPCC Core Writing Team, 2014), we find that an increase of  $>230 \mu\text{atm}$  ( $\sim 0.4$  doublings) would be very unlikely (i.e.,  $<5\%$  chance, see Figure S7). Reconciling this small a magnitude of  $p\text{CO}_2$  change with warming of  $\sim 3^\circ\text{C}$ , we suggest, would require one (or a combination of) (a) very high climate sensitivity to  $\text{CO}_2$  in the middle Eocene and/or some non- $\text{CO}_2$  climate forcing, (b) dynamic changes in ocean alkalinity that we do not properly account for during the onset of the MECO, or (c) a nonthermal (i.e., ice volume) component to carbonate  $\delta^{18}\text{O}$  change.

While calculating a precise estimate of climate sensitivity is difficult given the limited spatial coverage of available surface temperature records, the observed  $\sim 0.5\%$  decrease in benthic foraminiferal  $\delta^{18}\text{O}$  values could equate to  $\sim 2^\circ\text{C}$  global mean surface temperature change using the relationships for the pre-Pleistocene described by Hansen, Sato, Russell, and Kharecha (2013), assuming no ice volume component. Using our upper limit of 0.3  $\text{CO}_2$  doublings during the MECO onset, we would estimate an Earth system sensitivity of  $>6.7^\circ\text{K}$  per  $\text{CO}_2$  doubling. Such sensitivity would be far higher than model estimates of equilibrium climate sensitivity (IPCC Core Writing Team, 2014) and well outside of the range of climate sensitivities previously calculated over the Cenozoic (Rohling & Members, 2012). Moreover, any such heightened climate sensitivity would have to have lowered again at the peak MECO; otherwise, a 0.65 doubling of  $p\text{CO}_2$  would have produced  $>4^\circ\text{C}$  of warming on top of the gradual MECO warming trend, something which is not observed in marine temperature records.

Large-scale changes in ocean alkalinity are another hypothetical candidate for raising atmospheric  $\text{CO}_2$  without detectable change in surface pH (and thus foraminiferal  $\delta^{11}\text{B}$ ) during the MECO onset. A reduction in surface ocean TALK might be possible over the MECO interval if there were a reduction in silicate weathering, as suggested by Os isotopes and the observed shallowing of the CCD (van der Ploeg et al., 2018). However, without a concurrent reduction in DIC, such a scenario would be associated also with a reduction in global surface ocean pH, for which we see little evidence. For surface ocean aqueous  $p\text{CO}_2$ , and hence atmospheric  $p\text{CO}_2$ , to have risen without significant pH change, TALK and dissolved inorganic carbon (DIC) would have had to rise in a ratio of approximately 1:0.9. A process (or processes) by which such stoichiometry would arise is unclear and might necessitate a complex combination of weathering fluxes and organic carbon burial fluxes. However, all else being equal, such a rise in ocean TALK and DIC would have increased deep ocean carbonate saturation state, counter to observed MECO CCD change indicative of decreased saturation. Moreover, alkalinity would have to increase by  $\sim 1,000 \mu\text{mol/kg}$  and [DIC] by  $\sim 900 \mu\text{mol/kg}$  to increase  $p\text{CO}_2$  by  $300 \mu\text{atm}$ : magnitudes which seem unfeasibly large to reconcile with a lack of pronounced shift in  $\delta^{13}\text{C}$ . Thus, while possible factors controlling alkalinity such as dynamic changes in calcification fluxes (Boudreau et al., 2018; Henehan, Hull, et al., 2016) or sulfide oxidation (Calmels et al., 2014; Torres et al., 2017) merit further investigation with more complex earth system models, at this stage, it seems difficult to decouple pH and  $p\text{CO}_2$  during the MECO onset given the constraints of the marine carbonate cycle.

Alternatively, it is possible that there was some contribution from ice melt to the trend toward more negative  $\delta^{18}\text{O}$  during the MECO onset, as has been hypothesized elsewhere (e.g., Lyle et al., 2005; Tripathi et al., 2005). Besides amplifying changes in carbonate  $\delta^{18}\text{O}$ , ice growth and subsequent melt can also provide a mechanism to explain CCD change, by changing the balance of carbonate burial onto shelves versus the deep sea through sea level fluctuation (Lyle et al., 2005; Sluijs et al., 2013). As yet, however, evidence for earlier, pre-MECO glaciation is only suggestive and not conclusive. Certainly, some high-latitude influence on climate and carbon cycle at this time is evidenced by a strengthened influence of obliquity in climate records (Bosboom et al., 2014; Westerhold et al., 2014). Furthermore, the second “MECO-like” event shown in Figure 1 does roughly coincide with a known ephemeral Antarctic glaciation event at  $\sim 37.3$  Ma (Scher et al., 2014, and references within), perhaps by analogy lending some suggestive support for dynamic ice also around the MECO. A steeper slope in the relationship between high-latitude  $\text{TEX}_{86}$  and  $\delta^{18}\text{O}$  in the middle Eocene compared to the early Eocene (Bijl et al., 2009) and comparison of Mg/Ca and  $\delta^{18}\text{O}$  (Billups & Schrag, 2003; Dawber & Tripathi, 2011; Lear, 2000) could also support an additive nonthermal component to seawater  $\delta^{18}\text{O}$  fluctuations beginning prior to the MECO. Furthermore, although glaciation thresholds are highly

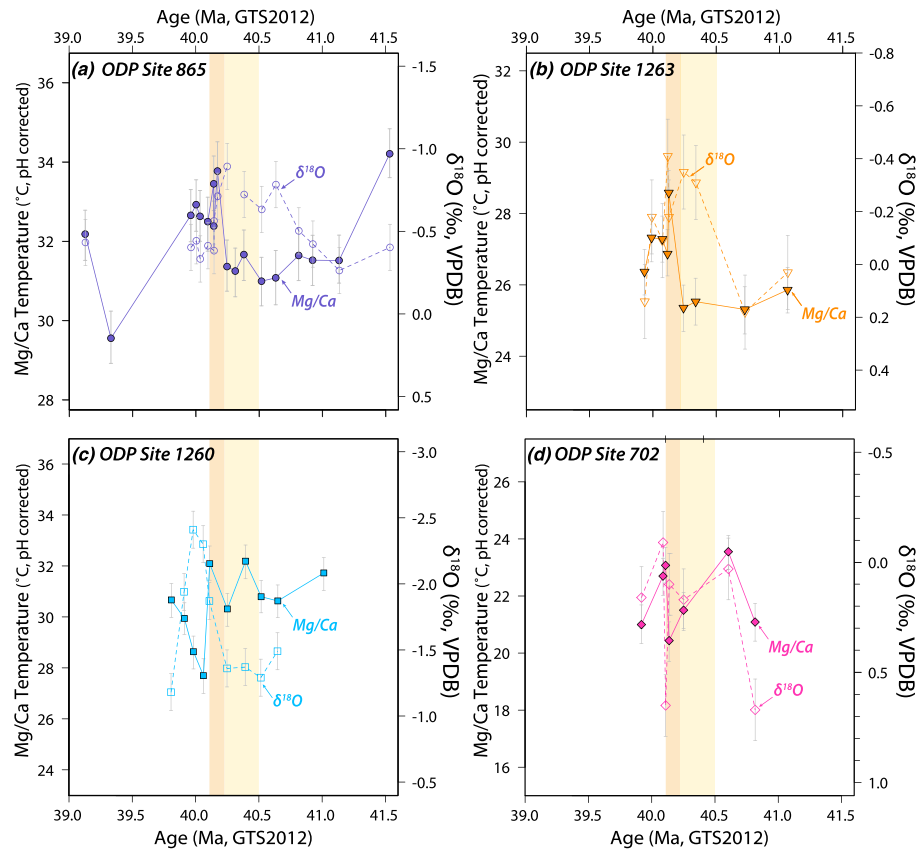


**Figure 9.** Mg/Ca-derived temperatures and oxygen isotope ratios across the MECO (a–d). Note that these data are derived from subsamples of the same crushed foraminifera measured for  $\delta^{11}\text{B}$ . While two sites (panels a and b) do show a decoupling of  $\delta^{18}\text{O}$  and Mg/Ca temperatures consistent with ice melt, two other sites do not (panels c and d). Site 1260 is particularly difficult to explain and may well reflect the influence locally of secondary controls on one or both of the proxies.

model-specific (Gasson et al., 2014), most general circulation models (GCMs) simulate some continental ice on Antarctica (e.g., DeConto & Pollard, 2003; Gasson et al., 2014) at pre-MECO  $p\text{CO}_2$  (e.g., Anagnostou et al., 2016). Temperature proxy records from the distal Antarctic peninsula (paleolatitude  $\sim 70^\circ$ ; van Hinsbergen et al., 2015) indicate coastal mean annual temperatures of  $\sim 10\text{--}15^\circ\text{C}$  prior to the MECO (Douglas et al., 2014; Judd et al., 2019), which when scaled to the continental interior should have been sufficiently cold to prompt glacial inception in the Gamburtsev mountains (Rose et al., 2013). Additionally, various lines of sedimentological, micropaleontological, and seismographic evidence (of varying degrees of certitude) exist for alpine or marine-terminating glaciers on Antarctica prior to or around the MECO (e.g., Birkenmajer, 1991; Ehrmann & Mackensen, 1992; Eitrem et al., 1995; Gulick et al., 2017; Margolis & Kennett, 1970), although we note that recently some of these interpretations of seismic features have been contested (Sauermilch et al., 2019). Further, while we stress that extensive northern hemisphere ice sheets were not present (Edgar et al., 2007), indicators for middle Eocene Arctic sea ice (Darby, 2014; Eldrett et al., 2007; Stickley et al., 2009; Tripathi et al., 2008) would seem incongruous with an ice-free Antarctic interior. Finally, the onset of synchronous changes in inferred sea level and  $\delta^{18}\text{O}$  (Browning et al., 1996; Dawber et al., 2011; Pekar et al., 2005) that follow 1.2 Myr obliquity cycles (Boulila et al., 2011) coincides with an inflection in the relationship between estimated sea level and global deep-sea temperatures around 42–44 Ma (Gasson et al., 2012; Kominz et al., 2008; Lear, 2000) that would also support ice volume change. We note though that this is strongly reliant on Kominz et al.'s New Jersey margin sea level reconstruction being representative of global eustasy (Gasson et al., 2012), and in such marginal marine settings, it is difficult to confidently distinguish global eustatic change from steric effects or sediment supply, especially given the flatter shelves likely present at this time (Sømme et al., 2009). In

sum, then, possible contributions from dynamic ice in driving middle Eocene  $\delta^{18}\text{O}$ ,  $\delta^{13}\text{C}$ , and CCD oscillations remain an open question but would help to explain some features of the event.

If middle Eocene ice reservoirs were present and were sensitive to orbital configuration, changes in ocean circulation, or small rises in  $p\text{CO}_2$ , ice melt during the MECO onset would have lowered  $\delta^{18}\text{O}_{\text{sw}}$  and raised sea level, and partitioned more carbonate deposition onto flooded shelves and away from the deep ocean (Lyle et al., 2005; Sluijs et al., 2013; Tripathi et al., 2005). Such a scenario could therefore reconcile our observed stable surface ocean pH, shoaling CCD and a decline in carbonate  $\delta^{18}\text{O}$  during the MECO onset. On one hand our new estimates of pre-MECO  $p\text{CO}_2$  fall well below most modeled thresholds required for significant Antarctic glaciation (although model dependent; Gasson et al., 2014), and evidence for sizeable glacio-eustatic fluctuations around this time (e.g., Browning et al., 1996) suggests this is not wholly unreasonable. On the other hand, as previously discussed, conclusive evidence for substantial middle Eocene ice reservoirs is still lacking. Furthermore, if the  $\delta^{18}\text{O}$  of pre-MECO ice was similar to Antarctic ice at the Eocene-Oligocene transition ( $\sim 34$  Ma), when ice growth increased global  $\delta^{18}\text{O}$  by  $0.6 \pm 0.15\text{‰}$ , if 0.4–0.5‰ (roughly half) of the global MECO  $\delta^{18}\text{O}$  decrease were attributable to ice, pre-MECO ice volumes available to melt would have had to be sizeable (equivalent to  $\sim 50$  m of sea level). Such a large change is most likely unrealistic, and indeed, our new Mg/Ca-based sea surface temperatures of  $>20$  °C (Figure 8) from ODP Site 702 at a paleolatitude of 55–60 °C (van Hinsbergen et al., 2015) seem hard to reconcile with such large volumes of ice. At this point, then, neither extreme Earth system sensitivity nor unstable, large middle Eocene ice reservoirs can be unequivocally ruled out.

A prediction of the ice melt hypothesis for the MECO onset is that other temperature proxies would show limited warming even as  $\delta^{18}\text{O}$  was declining. Although any one site may of course be subject to local hydrographic changes, globally, a sizeable secular  $\delta^{18}\text{O}_{\text{sw}}$  decline should be evident. For our part, we can compare  $\delta^{18}\text{O}$  and Mg/Ca-derived temperatures measured in the same samples of planktic foraminifera (Figure 9). At Sites 865 and 1263, which includes our highest resolution site, there is indeed a marked decline in  $\delta^{18}\text{O}$  before any change in Mg/Ca. However, at Site 702, Mg/Ca and  $\delta^{18}\text{O}$  are more or less in-step, while at Site 1260, Mg/Ca shows no response with declining  $\delta^{18}\text{O}$  values but indicates a sharp cooling at the peak. Published organic biomarker temperature proxies ( $\text{TEX}_{86}$  and  $\text{U}^k_{37}$ ) should allow another means to test this hypothesis. In support of an elevated Earth system sensitivity scenario, bulk carbonate  $\delta^{18}\text{O}$  and organic temperature proxies at ODP Site 1172 move more or less in unison (Bijl et al., 2010) during the period in which we see little change in global ocean pH. Lower-resolution  $\text{TEX}_{86}$  data over the MECO at nearby ODP Site 1170 also show MECO warmth, albeit more muted (Cramwinckel et al., 2019). However, a possible incursion of the warm East-Australian current into this area around the MECO is indicated by fossil assemblages (Cramwinckel, Woelders, et al., 2019), which may complicate these signals. At equatorial ODP Site 959 a clear MECO warming event is expressed in  $\text{TEX}_{86}$  (Cramwinckel et al., 2018), but differing sample resolution makes it difficult to discern how clear the correlation between bulk carbonate  $\delta^{18}\text{O}$  and  $\text{TEX}_{86}$  is at this site (Cramwinckel et al., 2019). Additionally, a lack of age model tie points between 40.02 and 42.84 Ma at this site makes it difficult to definitively discern whether the warming expressed in  $\text{TEX}_{86}$  was gradual and began during the global MECO onset or was rapid and focused around the peak MECO, when our boron isotope data indicate  $\text{CO}_2$  rise. Finally, at ODP Site 1263, there is no apparent correlation between  $\text{TEX}_{86}$  and concurrent carbonate  $\delta^{18}\text{O}$  values (Boscolo Galazzo et al., 2014). As yet, then, evidence is not sufficiently conclusive to definitively accept or reject the hypothesis of ice melt contribution to  $\delta^{18}\text{O}$  change during the onset of the MECO. However, the extremely high climate sensitivity to  $p\text{CO}_2$  otherwise implied by our boron data suggests that a component of ice melt is a hypothesis worthy of further interrogation.

#### 4.2. Caveats, Conclusions, and Prospects

By combining with LOSCAR simulations, we derive boron-based estimates of  $p\text{CO}_2$  between 40.21–41.0 Ma of  $\sim 550$   $\mu\text{atm}$  ( $2\sigma_{-80}^{+110}$   $\mu\text{atm}$ ; see Figure S6) that provide a precise estimate of the boundary conditions on which the MECO was superimposed. Additionally, our estimate of peak MECO  $p\text{CO}_2$  of  $\sim 870$   $\mu\text{atm}$  ( $2\sigma_{-100}^{+130}$   $\mu\text{atm}$ ; see Figure S6) tightly constrains  $\text{CO}_2$  forcing change ( $\Delta F$ ) to between 2.3 and 2.5  $\text{W m}^{-2}$  (Figure 8c). These data confirm the finding of Bijl et al. (2010) that there was a rise in  $p\text{CO}_2$  over the

MECO, albeit to a lower degree and superimposed upon a lower baseline  $p\text{CO}_2$  than indicated by the alkenone  $\delta^{13}\text{C}$ - $p\text{CO}_2$  proxy. A number of outstanding puzzles surrounding the MECO clearly remain, however. The question of reduced silicate weathering at the MECO (van der Ploeg et al., 2018) remains open, for example, and requires further investigation. A reduced silicate weathering feedback would have implications for our LOSCAR-derived  $p\text{CO}_2$  estimates, in that we use default configuration weathering in LOSCAR to predict the evolution of TALK expected over the course of a 100 kyr  $\text{CO}_2$  injection, allowing us to convert pH to  $p\text{CO}_2$ . As demonstrated in Figure 7, the effect of a reduced silicate weathering feedback over the MECO would be to necessitate a smaller mass of  $\text{CO}_2$  to be input to effect the same change in ocean pH and  $\delta^{11}\text{B}$ . However, there are a number of reasons why we do not attempt to explore this in greater depth with LOSCAR here. First, while a temporarily weakened and subsequently reactivated silicate weathering feedback is an elegant hypothesis, it is not the only solution that could explain changes in Os isotopes and changes in CCD. For example, rising sea level could conceivably partition more carbonate deposition onto shelves and shoal the CCD (as already demonstrated in LOSCAR; Sluijs et al., 2013) while simultaneously changing the relative contributions of radiogenic versus nonradiogenic rocks to global weathering fluxes. Effects on marine Si cycling, an often-overlooked implication of mechanisms that invoke a dynamic silicate weathering feedback, could provide an independent means to interrogate the hypothesis of reduced silicate weathering at the MECO. During earlier Paleocene and Eocene warming events, the silicate weathering feedback on land drove enhanced burial and preservation of biogenic silica in the oceans as Si input fluxes were elevated (Penman, 2016; Penman et al., 2019). By analogy, a weakened silicate weathering feedback prior to the MECO might predict reduced burial of silica in the middle Eocene ocean. However, opal mass accumulation rates in the Pacific were among their highest Eocene levels in radiolarian zones RP14 and RP15, preceding the MECO (Moore et al., 2008). Moreover, the response to the MECO in the North Atlantic (Witkowski et al., 2014), the Southern Ocean (Witkowski et al., 2012), and the equatorial Indian Ocean (Savain et al., 2016) was a pronounced rise in the deposition/preservation of siliceous plankton, supportive perhaps of a global rise in marine [Si] concurrent with warming. These records do not therefore immediately appear consistent with a weakened silicate weathering feedback at the MECO. However, we would encourage further investigation into the magnitude and geographical extent of this enhanced silica burial and to look for chert deposits analogous to those seen after earlier warming events (Penman, 2016; Penman et al., 2019) to independently test the weakened silicate weathering hypothesis. Furthermore, interrogating other weathering-sensitive isotope systems such as Li, Si, or Sr may help in further constraining changes in silicate weathering over this event.

Besides questions over the dynamics of the silicate weathering feedback, we suggest that even implementing a weakened and then restored silicate weathering feedback in LOSCAR (as in van der Ploeg et al., 2018) would not fully capture the complexity of the MECO event. In such simulations (e.g., Sluijs et al., 2013; van der Ploeg et al., 2018)  $\text{CO}_2$  drawdown is not as rapid as the recovery of pH and global temperatures observed after the MECO and is usually accompanied by an overshoot in simulated CCD, for which (at least in the Pacific and Indian Oceans) there is scant sedimentary evidence. This may suggest a role for organic matter burial (Moebius et al., 2015; Spofforth et al., 2010) and/or ocean carbon storage (Sexton et al., 2011). To simulate these forcings realistically, and to accurately reproduce MECO surface ocean  $\delta^{13}\text{C}$  changes (which vary widely both in magnitude and direction of change globally), would require a more complex model with dynamic ocean circulation. In short it is likely that during the MECO and its recovery more complex biogeochemical feedbacks were at work than are represented in the LOSCAR simulations of Sluijs et al. (2013), Van der Ploeg (2018), or our current contribution. Therefore, we present our scenarios for MECO  $p\text{CO}_2$  change as current best estimates, mindful that lower TALK change due to weakened silicate weathering might reduce the required mass of C injection but that higher sampling resolution around the short pH minimum (statistically underweighted in our global LOESS as it is defined by a single data point) might increase it.

In summary, these data offer robust independent confirmation of  $p\text{CO}_2$  rise during the MECO, the bulk of which occurs at the peak of the 400 kyr event. Although our new  $p\text{CO}_2$  estimates do not allow us to ascertain the causal driver of the MECO, a number of informative observations can be made. First, the mass of C that was transferred to and from the surface ocean-atmosphere system over the MECO was considerably smaller than that required to explain previous MECO  $\Delta p\text{CO}_2$  estimates based on the alkenone  $\delta^{13}\text{C}$  proxy (Bijl et al., 2010), and if the silicate weathering feedback were diminished, this mass could be smaller still.

This smaller mass could bring internal reorganization of carbon reservoirs into play in explaining the MECO, rather than invoking a large exogenous carbon injection. Second, the limited evidence we see globally for any substantial rise in  $p\text{CO}_2$  during the onset stage of the MECO suggests a climate, and perhaps nascent cryosphere, that was highly sensitive to perturbation. While we suggest that a contribution to global  $\delta^{18}\text{O}$  change from ice melt during the initial phase of the MECO may be the most parsimonious means to reconcile CCD shoaling and limited  $p\text{CO}_2$  rise, we recognize that further work is required to ascertain the feasibility of such a scenario. For instance, more precise dating of glacial deposits and more extensive circum-Antarctic temperature proxy records are of vital importance. Furthermore, we encourage further comparison of  $\delta^{18}\text{O}$  with concurrent independent temperature proxies (e.g.,  $\text{TEX}_{86}$  and clumped isotopes) to further isolate  $\delta^{18}\text{O}_{\text{sw}}$  change over the MECO. Modeling work to explore the potential  $\delta^{18}\text{O}$  range of nascent middle Eocene ice would also be beneficial, to constrain the volumes of ice melt required. Finally, while a trigger for ice melt without significant  $p\text{CO}_2$  rise is uncertain, we suggest that ocean circulation is a prime target for investigation, given (a) spatially variable bulk carbonate  $\delta^{13}\text{C}$  changes (Bohaty et al., 2009), (b) spatial variability in circum-Antarctic temperature (Douglas et al., 2014; Judd et al., 2019), (c) geochemical and micropaleontological evidence for changing high-latitude ocean circulation (Cramwinckel, Woelders, et al., 2019; Scher & Delaney, 2010), and (d) enhanced sensitivity of global thermohaline circulation to orbital configuration (Vahlenkamp et al., 2018) around the MECO. In sum, while our new estimates of  $p\text{CO}_2$  across the MECO move our understanding of this event forward, there remains considerable work to be done to fully elucidate the drivers of this enigmatic event.

#### Acknowledgments

This research used samples provided by the International Ocean Discovery Program (IODP). We thank Steve Bohaty for assistance with stratigraphy, provision of sample material from Sites 702 and 1263, and helpful discussion. We thank Paul Wilson for providing access to washed sample residues for Sites 1260. We thank Paige Breen for providing  $\delta^{13}\text{C}$  and  $\delta^{18}\text{O}$  data from IODP Site 1408. We thank Tom Chalk for assistance with trace element analysis and the rest of the B-Team at the University of Southampton for their help and cooperation. We thank Bärbel Hönlisch, Christopher Pearce, David Evans, and Mathis Hain for helpful discussion and Ellen Thomas for providing feedback on an earlier draft of the manuscript. We also thank Peter Bijl and one anonymous reviewer for helpful feedback which improved the manuscript. Financial support was provided from via the Yale Peabody Museum to M. J. H., a NERC Postdoctoral Research Fellowship (NE/H016457/1), NERC Standard Grant (NE/P013112/1) and Leverhulme Early Career Fellowship (ECF-2013-608) to K. M. E., a Flint Postdoctoral Fellowship to D. E. P., and NERC grants awarded to P. N. P. (NE/I005870/1) and G. L. F. (NE/I005595/1). We report no conflicts of interests for any coauthors. All data supporting our conclusions are available in the supporting information and is also archived on PANGAEA (<https://doi.pangaea.de/10.1594/PANGAEA.909432>).

#### References

- Abels, H. A., Clyde, W. C., Gingerich, P. D., Hilgen, F. J., Fricke, H. C., Bowen, G. J., & Lourens, L. J. (2012). Terrestrial carbon isotope excursions and biotic change during Palaeogene hyperthermals. *Nature Geoscience*, *5*(5), 326–329. <https://doi.org/10.1038/ngeo1427>
- Anagnostou, E., John, E. H., Edgar, K. M., Foster, G. L., Ridgwell, A., Inglis, G. N., et al. (2016). Changing atmospheric  $\text{CO}_2$  concentration was the primary driver of early Cenozoic climate. *Nature*, *533*(7603), 380–384. <https://doi.org/10.1038/nature17423>
- Arreguin-Rodríguez, G. J., Alegret, L., & Thomas, E. (2016). Late Paleocene-middle Eocene benthic foraminifera on a Pacific seamount (Allison Guyot, ODP Site 865): Greenhouse climate and superimposed hyperthermal events: Benthic foraminifera on Pacific seamount. *Paleoceanography*, *31*, 346–364. <https://doi.org/10.1002/2015PA002837>
- Barnet, J. S. K., Littler, K., Kroon, D., Leng, M. J., Westerhold, T., Röhl, U., & Zachos, J. C. (2018). A new high-resolution chronology for the late Maastrichtian warming event: Establishing robust temporal links with the onset of Deccan volcanism. *Geology*, *46*(2), 147–150. <https://doi.org/10.1130/G39771.1>
- Barnet, J. S. K., Littler, K., Westerhold, T., Kroon, D., Leng, M. J., Bailey, I., et al. (2019). A high-fidelity benthic stable isotope record of late Cretaceous–Early Eocene climate change and carbon-cycling. *Paleoceanography and Paleoclimatology*, *34*, 672–691. <https://doi.org/10.1029/2019PA003556>
- Ben-Yaakov, S., & Goldhaber, M. B. (1973). The influence of sea water composition on the apparent constants of the carbonate system. *Deep Sea Research and Oceanographic Abstracts*, *20*(1), 87–99. [https://doi.org/10.1016/0011-7471\(73\)90044-2](https://doi.org/10.1016/0011-7471(73)90044-2)
- Benyamovskiy, V. N. (2012). A high resolution Lutetian-Bartonian planktonic foraminiferal zonation in the Crimean-Caucasus region of the northeastern Peri-Tethys. *Austrian Journal of Earth Sciences*, *105*(1), 117–128.
- Berner, R. A., Lasaga, A. C., & Garrels, R. M. (1983). The carbonate-silicate geochemical cycle and its effect on atmospheric carbon dioxide over the past 100 million years. *American Journal of Science*, *283*(7), 641–683. <https://doi.org/10.2475/ajs.283.7.641>
- Bijl, P. K., Houben, A. J. P., Schouten, S., Bohaty, S. M., Sluijs, A., Reichert, G. J., et al. (2010). Transient Middle Eocene atmospheric  $\text{CO}_2$  and temperature variations. *Science*, *330*(6005), 819–821. <https://doi.org/10.1126/science.1193654>
- Bijl, P. K., Schouten, S., Sluijs, A., Reichert, G.-J., Zachos, J. C., & Brinkhuis, H. (2009). Early Palaeogene temperature evolution of the southwest Pacific Ocean. *Nature*, *461*(7265), 776–779. <https://doi.org/10.1038/nature08399>
- Billups, K., & Schrag, D. P. (2003). Application of benthic foraminiferal Mg/Ca ratios to questions of Cenozoic climate change. *Earth and Planetary Science Letters*, *209*(1–2), 181–195. [https://doi.org/10.1016/S0012-821X\(03\)00067-0](https://doi.org/10.1016/S0012-821X(03)00067-0)
- Birch, H. S., Coxall, H. K., & Pearson, P. N. (2012). Evolutionary ecology of Early Paleocene planktonic foraminifera: Size, depth habitat and symbiosis. *Paleobiology*, *38*(3), 374–390. <https://doi.org/10.1666/11027.1>
- Birkenmajer, K. (1991). Tertiary glaciation in the South Shetland Islands, West Antarctica: Evaluation of data. In M. R. A. Thomson, J. A. Crame, & J. W. Thomson (Eds.), *Geological evolution of Antarctica* (pp. 629–632). Cambridge, UK: Cambridge Univ. Press.
- Bohaty, S. M., & Zachos, J. C. (2003). Significant Southern Ocean warming event in the late middle Eocene. *Geology*, *31*(11), 1017–1020. <https://doi.org/10.1130/G19800.1>
- Bohaty, S. M., Zachos, J. C., Florindo, F., & Delaney, M. L. (2009). Coupled greenhouse warming and deep-sea acidification in the middle Eocene. *Paleoceanography*, *24*, PA2207. <https://doi.org/10.1029/2008PA001676>
- Bosboom, R. E., Abels, H. A., Hoorn, C., van den Berg, B. C. J., Guo, Z., & Dupont-Nivet, G. (2014). Aridification in continental Asia after the Middle Eocene Climatic Optimum (MECO). *Earth and Planetary Science Letters*, *389*, 34–42. <https://doi.org/10.1016/j.epsl.2013.12.014>
- Boscolo Galazzo, F., Thomas, E., & Giusberti, L. (2015). Benthic foraminiferal response to the Middle Eocene Climatic Optimum (MECO) in the south-eastern Atlantic (ODP Site 1263). *Palaeogeography, Palaeoclimatology, Palaeoecology*, *417*, 432–444. <https://doi.org/10.1016/j.palaeo.2014.10.004>
- Boscolo Galazzo, F., Thomas, E., Pagani, M., Warren, C., & Giusberti, L. (2014). The middle Eocene climatic optimum (MECO): A multiproxy record of paleoceanographic changes in the southeast Atlantic (ODP Site 1263, Walvis Ridge): MECO repercussions in the SE Atlantic. *Paleoceanography*, *29*, 1143–1161. <https://doi.org/10.1002/2014PA002670>

- Boudreau, B. P., Middelburg, J. J., & Luo, Y. (2018). The role of calcification in carbonate compensation. *Nature Geoscience*, *11*(12), 894–900. <https://doi.org/10.1038/s41561-018-0259-5>
- Boullia, S., Galbrun, B., Miller, K. G., Pekar, S. F., Browning, J. V., Laskar, J., & Wright, J. D. (2011). On the origin of Cenozoic and Mesozoic “third-order” eustatic sequences. *Earth-Science Reviews*, *109*(3–4), 94–112. <https://doi.org/10.1016/j.earscirev.2011.09.003>
- Bralower, T. J., Zachos, J. C., Thomas, E., Parrow, M., Paull, C. K., Kelly, D. C., Silva, I. P., Sliter, W. V., & Lohmann, K. C. (1995). Late Paleocene to Eocene paleoceanography of the equatorial Pacific Ocean: Stable isotopes recorded at Ocean Drilling Program Site 865, Allison Guyot. *Paleoceanography*, *10*(4), 841–865. <https://doi.org/10.1029/95PA01143>
- Browning, J. V., Miller, K. G., & Pak, D. K. (1996). Global implications of lower to middle Eocene sequence boundaries on the New Jersey coastal plain: The icehouse cometh. *Geology*, *24*(7), 639. [https://doi.org/10.1130/0091-7613\(1996\)024<0639:GIOLTM>2.3.CO;2](https://doi.org/10.1130/0091-7613(1996)024<0639:GIOLTM>2.3.CO;2)
- Calmels, D., Gaillardet, J., & François, L. (2014). Sensitivity of carbonate weathering to soil CO<sub>2</sub> production by biological activity along a temperate climate transect. *Chemical Geology*, *390*, 74–86. <https://doi.org/10.1016/j.chemgeo.2014.10.010>
- Clement, B. M., & Hailwood, E. A. (1991). Magnetostratigraphy of sediments from Sites 701 and 702. In P. F. Cieselski, Y. Kristoffersen, et al. (Eds.), *Proceedings of the Ocean Drilling Program: Scientific Results*, (Vol. 114, pp. 359–366). College Station, TX: Ocean Drilling Program.
- Colbourn, G., Ridgwell, A., & Lenton, T. M. (2015). The time scale of the silicate weathering negative feedback on atmospheric CO<sub>2</sub>. *Global Biogeochemical Cycles*, *29*, 583–596. <https://doi.org/10.1002/2014GB005054>
- Core Team, R. (2015). *R: A language and environment for statistical computing*. Vienna, Austria: R Foundation for Statistical Computing. Retrieved from [www.R-project.org](http://www.R-project.org)
- Cramer, B. S., Toggweiler, J. R., Wright, J. D., Katz, M. E., & Miller, K. G. (2009). Ocean overturning since the Late Cretaceous: Inferences from a new benthic foraminiferal isotope compilation. *Paleoceanography*, *24*, PA4216. <https://doi.org/10.1029/2008PA001683>
- Cramwinckel, M. J., Huber, M., Kocken, I. J., Agnini, C., Bijl, P. K., Bohaty, S. M., et al. (2018). Synchronous tropical and polar temperature evolution in the Eocene. *Nature*, *559*(7714), 382–386. <https://doi.org/10.1038/s41586-018-0272-2>
- Cramwinckel, M. J., van der Ploeg, R., Bijl, P. K., Peterse, F., Bohaty, S. M., Röhl, U., et al. (2019). Harmful algae and export production collapse in the equatorial Atlantic during the zenith of Middle Eocene Climatic Optimum warmth. *Geology*, *47*(3), 247–250. <https://doi.org/10.1130/G45614.1>
- Cramwinckel, M. J., Woelders L., Huurdeman E. P., Peterse F., Gallagher S. J., Pross J., et al. (2019). Surface-circulation change in the Southern Ocean across the Middle Eocene Climatic Optimum: Inferences from dinoflagellate cysts and biomarker paleothermometry. *Climate of the Past Discussions*, 1–34. <https://doi.org/10.5194/cp-2019-35>
- D'Hondt, S., Zachos, J. C., & Schultz, G. (1994). Stable isotopic signals and photosymbiosis in Late Paleocene planktic foraminifera. *Paleobiology*, *20*(03), 391–406. <https://doi.org/10.1017/S0094837300012847>
- Darby, D. A. (2014). Ephemeral formation of perennial sea ice in the Arctic Ocean during the middle Eocene. *Nature Geoscience*, *7*(3), 210–213. <https://doi.org/10.1038/ngeo2068>
- Dawber, C. F., & Tripathi, A. K. (2011). Constraints on glaciation in the middle Eocene (46–37 Ma) from Ocean Drilling Program (ODP) Site 1209 in the tropical Pacific Ocean: GLACIATION IN THE MIDDLE EOCENE. *Paleoceanography*, *26*, PA2208. <https://doi.org/10.1029/2010PA002037>
- Dawber, C. F., Tripathi, A. K., Gale, A. S., MacNiocaill, C., & Hesselbo, S. P. (2011). Glacioeustasy during the middle Eocene? Insights from the stratigraphy of the Hampshire Basin, UK. *Palaeogeography, Palaeoclimatology, Palaeoecology*, *300*(1–4), 84–100. <https://doi.org/10.1016/j.palaeo.2010.12.012>
- DeConto, R. M., & Pollard, D. (2003). Rapid Cenozoic glaciation of Antarctica induced by declining atmospheric CO<sub>2</sub>. *Nature*, *421*(6920), 245–249. <https://doi.org/10.1038/nature01290>
- Dickens, G. R., O'Neil, J. R., Rea, D. K., & Owen, R. M. (1995). Dissociation of oceanic methane hydrate as a cause of the carbon isotope excursion at the end of the Paleocene. *Paleoceanography*, *10*(6), 965–971. <https://doi.org/10.1029/95PA02087>
- Douglas, P. M. J., Affek, H. P., Ivany, L. C., Houben, A. J. P., Sijp, W. P., Sluijs, A., et al. (2014). Pronounced zonal heterogeneity in Eocene southern high-latitude sea surface temperatures. *Proceedings of the National Academy of Sciences*, *111*(18), 6582–6587. <https://doi.org/10.1073/pnas.1321441111>
- Edgar, K. M., Anagnostou, E., Pearson, P. N., & Foster, G. L. (2015). Assessing the impact of diagenesis on  $\delta^{11}\text{B}$ ,  $\delta^{13}\text{C}$ ,  $\delta^{18}\text{O}$ , Sr/Ca and B/Ca values in fossil planktic foraminiferal calcite. *Geochimica et Cosmochimica Acta*, *166*, 189–209. <https://doi.org/10.1016/j.gca.2015.06.018>
- Edgar, K. M., Bohaty, S. M., Coxall, H. K., Bown, P. R., Batenburg, S. J., Lear, C. H., & Pearson, P. N. (subm.). New composite section with bio- and isotope stratigraphies spanning the Middle Eocene Climatic Optimum from tropical ODP Site 865 in the Pacific Ocean. <https://doi.org/10.31223/osf.io/m64gk>
- Edgar, K. M., Bohaty, S. M., Gibbs, G., Samantha, J., Sexton, P. F., Norris, R. D., & Wilson, P. A. (2013). Symbiotic ‘bleaching’ in planktic foraminifera during the Middle Eocene Climatic Optimum. *Geology*, *41*(1), 15–18. <https://doi.org/10.1130/G33388.1>
- Edgar, K. M., Wilson, P. A., Sexton, P. F., Gibbs, S. J., Roberts, A. P., & Norris, R. D. (2010). New biostratigraphic, magnetostratigraphic and isotopic insights into the Middle Eocene Climatic Optimum in low latitudes. *Palaeogeography, Palaeoclimatology, Palaeoecology*, *297*(3–4), 670–682. <https://doi.org/10.1016/j.palaeo.2010.09.016>
- Edgar, K. M., Wilson, P. A., Sexton, P. F., & Sugauma, Y. (2007). No extreme bipolar glaciation during the main Eocene calcite compensation shift. *Nature*, *448*(7156), 908–911. <https://doi.org/10.1038/nature06053>
- Ehrmann, W. U., & Mackensen, A. (1992). Sedimentological evidence for the formation of an East Antarctic ice sheet in Eocene/Oligocene time. *Palaeogeography, Palaeoclimatology, Palaeoecology*, *93*(1–2), 85–112. [https://doi.org/10.1016/0031-0182\(92\)90185-8](https://doi.org/10.1016/0031-0182(92)90185-8)
- Eitrem, S. L., Cooper, A. K., & Wannesson, J. (1995). Seismic stratigraphic evidence of ice-sheet advances on the Wilkes Land margin of Antarctica. *Sedimentary Geology*, *96*(1–2), 131–156. [https://doi.org/10.1016/0037-0738\(94\)00130-M](https://doi.org/10.1016/0037-0738(94)00130-M)
- Eldrett, J. S., Harding, I. C., Wilson, P. A., Butler, E., & Roberts, A. P. (2007). Continental ice in Greenland during the Eocene and Oligocene. *Nature*, *446*(7132), 176–179. <https://doi.org/10.1038/nature05591>
- Evans, D., Brierley, C., Raymo, M. E., Erez, J., & Müller, W. (2016). Planktic foraminifera shell chemistry response to seawater chemistry: Pliocene–Pleistocene seawater Mg/Ca, temperature and sea level change. *Earth and Planetary Science Letters*, *438*, 139–148. <https://doi.org/10.1016/j.epsl.2016.01.013>
- Evans, D., Wade, B. S., Henahan, M. J., Erez, J., & Müller, W. (2016). Revisiting carbonate chemistry controls on planktic foraminifera Mg/Ca: Implications for sea surface temperature and hydrology shifts over the Paleocene–Eocene thermal maximum and Eocene–Oligocene transition. *Climate of the Past*, *12*(4), 819–835. <https://doi.org/10.5194/cp-12-819-2016>
- Ezard, T. H. G., Edgar, K. M., & Hull, P. M. (2015). Environmental and biological controls on size-specific  $\delta^{13}\text{C}$  and  $\delta^{18}\text{O}$  in recent planktonic foraminifera. *Paleoceanography*, *30*, 151–173. <https://doi.org/10.1002/2014PA002735>

- Foster, G. L. (2008). Seawater pH, pCO<sub>2</sub> and [CO<sub>3</sub><sup>2-</sup>] variations in the Caribbean Sea over the last 130 kyr: A boron isotope and B/Ca study of planktic foraminifera. *Earth and Planetary Science Letters*, 271(1–4), 254–266. <https://doi.org/10.1016/j.epsl.2008.04.015>
- Foster, G. L., Lear, C. H., & Rae, J. W. B. (2012). The evolution of pCO<sub>2</sub>, ice volume and climate during the middle Miocene. *Earth and Planetary Science Letters*, 341–344, 243–254. <https://doi.org/10.1016/j.epsl.2012.06.007>
- Foster, G. L., & Rae, J. W. B. (2016). Reconstructing ocean pH with boron isotopes in foraminifera. *Annual Review of Earth and Planetary Sciences*, 44(1), 207–237. <https://doi.org/10.1146/annurev-earth-060115-012226>
- Gasson, E., Lunt, D. J., DeConto, R. M., Goldner, A., Heinemann, M., Huber, M., et al. (2014). Uncertainties in the modelled CO<sub>2</sub> threshold for Antarctic glaciation. *Climate of the Past*, 10(2), 451–466. <https://doi.org/10.5194/cp-10-451-2014>
- Gasson, E., Siddall, M., Lunt, D. J., Rackham, O. J. L., Lear, C. H., & Pollard, D. (2012). Exploring uncertainties in the relationship between temperature, ice volume, and sea level over the past 50 million years. *Reviews of Geophysics*, 50, RG1005. <https://doi.org/10.1029/2011RG000358>
- Golub, G. H., Heath, M., & Wahba, G. (1979). Generalized cross-validation as a method for choosing a good ridge parameter. *Technometrics*, 21(2), 215–223. <https://doi.org/10.1080/00401706.1979.10489751>
- Gradstein, F. M., Ogg, J. G., Schmitz, M., & Ogg, G. (2012). *The geologic time scale 2012 2-Volume Set*. Oxford, Amsterdam: Elsevier. <https://doi.org/10.1016/B978-0-444-59425-9>
- Gray, W. R., & Evans, D. (2019). Nonthermal Influences on Mg/Ca in planktonic foraminifera: A review of culture studies and application to the last glacial maximum. *Paleoceanography and Paleoclimatology*, 18, 1050. <https://doi.org/10.1029/2018PA003517>
- Greenop, R., Hain, M. P., Sosdian, S., Oliver, K. I. C., Goodwin, P., Chalk, T. B., et al. (2017). A record of Neogene seawater δ<sup>11</sup>B reconstructed from paired δ<sup>11</sup>B analyses on benthic and planktic foraminifera. *Climate of the Past*, 13, 149–170. <https://doi.org/10.5194/cp-13-149-2017>
- Greenop, R., Sosdian, S. M., Henehan, M. J., Wilson, P. A., Lear, C. H., & Foster, G. L. (2019). Orbital forcing, ice volume, and CO<sub>2</sub> across the Oligocene-Miocene transition. *Paleoceanography and Paleoclimatology*, 34(3), 316–328. <https://doi.org/10.1029/2018PA003420>
- Gulick, S. P. S., Shevenell, A. E., Montelli, A., Fernandez, R., Smith, C., Warny, S., et al. (2017). Initiation and long-term instability of the East Antarctic ice sheet. *Nature*, 552(7684), 225–229. <https://doi.org/10.1038/nature25026>
- Gutjahr, M., Ridgwell, A., Sexton, P. F., Anagnostou, E., Pearson, P. N., Pälike, H., et al. (2017). Very large release of mostly volcanic carbon during the Palaeocene–Eocene thermal maximum. *Nature*, 548(7669), 573–577. <https://doi.org/10.1038/nature23646>
- Hain, M. P., Sigman, D. M., Higgins, J. A., & Haug, G. H. (2015). The effects of secular calcium and magnesium concentration changes on the thermodynamics of seawater acid/base chemistry: Implications for Eocene and Cretaceous ocean carbon chemistry and buffering. *Global Biogeochemical Cycles*, 28, 517–533. <https://doi.org/10.1002/2014GB004986>
- Hansen, J., Sato, M., Russell, G., & Kharecha, P. (2013). Climate sensitivity, sea level and atmospheric carbon dioxide. *Philosophical Transactions of the Royal Society A*, 371, 20120294. <https://doi.org/10.1098/rsta.2012.0294>
- Hay, W. W., DeConto, R. M., Wold, C. N., Wilson, K. M., Voigt, S., Schulz, M., et al. (1999). Alternative global Cretaceous paleogeography. In E. Barrera, & C. C. Johnson (Eds.), *The Evolution of Cretaceous ocean/climate systems*, (pp. 1–47). Boulder, CO: Geological Society of America. <https://doi.org/10.1130/0-8137-2332-9.1>
- Hemming, N. G., & Hanson, G. N. (1992). Boron isotopic composition and concentration in modern marine carbonates. *Geochimica et Cosmochimica Acta*, 56(1), 537–543. [https://doi.org/10.1016/0016-7037\(92\)90151-8](https://doi.org/10.1016/0016-7037(92)90151-8)
- Henehan, M. J., Foster, G. L., Bostock, H. C., Greenop, R., Marshall, B. J., & Wilson, P. A. (2016). A new boron isotope-pH calibration for *Orbulina universa*, with implications for understanding and accounting for ‘vital effects’. *Earth and Planetary Science Letters*, 454, 282–292. <https://doi.org/10.1016/j.epsl.2016.09.024>
- Henehan, M. J., Hull, P. M., Penman, D. E., Rae, J. W. B., & Schmidt, D. N. (2016). Biogeochemical significance of pelagic ecosystem function: An end-Cretaceous case study. *Philosophical Transactions of the Royal Society B*, 371, 20150510. <https://doi.org/10.1098/rstb.2015.0510>
- Henehan, M. J., Rae, J. W. B., Foster, G. L., Erez, J., Prentice, K. C., Kucera, M., et al. (2013). Calibration of the boron isotope proxy in the planktonic foraminifera *Globigerinoides ruber* for use in palaeo-CO<sub>2</sub> reconstruction. *Earth and Planetary Science Letters*, 364, 111–122. <https://doi.org/10.1016/j.epsl.2012.12.029>
- Hönisch, B., Allen, K. A., Lea, D. W., Spero, H. J., Eggins, S. M., Arbuszewski, J., et al. (2013). The influence of salinity on Mg/Ca in planktic foraminifers—Evidence from cultures, core-top sediments and complementary δ<sup>18</sup>O. *Geochimica et Cosmochimica Acta*, 121, 196–213. <https://doi.org/10.1016/j.gca.2013.07.028>
- Hönisch, B., Bijma, J., Russell, A. D., Spero, H. J., Palmer, M. R., Zeebe, R. E., & Eisenhauer, A. (2003). The influence of symbiotic photosynthesis on the boron isotopic composition of foraminifera shells. *Marine Micropaleontology*, 49(1–2), 87–96. [https://doi.org/10.1016/S0377-8398\(03\)00030-6](https://doi.org/10.1016/S0377-8398(03)00030-6)
- IPCC Core Writing Team (2014). *Climate Change 2014: Synthesis report. Contribution of Working Groups I, II and III to the Fifth Assessment Report of the Intergovernmental Panel on Climate Change*, (Vol. AR5, p. 151). Geneva, Switzerland: IPCC.
- Jørgensen, B. B., Erez, J., Revsbech, N. P., & Cohen, Y. (1985). Symbiotic photosynthesis in a planktonic Foraminiferan, *Globigerinoides sacculifer* (Brady), studied with microelectrodes. *Limnology and Oceanography*, 30(6), 1253–1267. <https://doi.org/10.4319/lo.1985.30.6.1253>
- Judd, E. J., Ivany, L. C., DeConto, R. M., Halberstadt, A. R. W., Miklus, N. M., Junium, C. K., & Uveges, B. T. (2019). Seasonally resolved proxy data from the Antarctic Peninsula support a heterogeneous middle Eocene Southern Ocean. *Paleoceanography and Paleoclimatology*, 34, 789–799. <https://doi.org/10.1029/2019PA003581>
- Katz, M. E., & Miller, K. G. (1991). Early Palaeogene benthic Foraminiferal assemblages and stable isotopes in the southern ocean. In *Proceedings of the Ocean Drilling Program* (Vol. 114, pp. 481–512). Texas: A&M University.
- Kelly, D. C., Zachos, J. C., Bralower, T. J., & Schellenberg, S. A. (2005). Enhanced terrestrial weathering/runoff and surface ocean carbonate production during the recovery stages of the Paleocene-Eocene thermal maximum: PETM negative feedback mechanisms. *Paleoceanography*, 20, PA4023. <https://doi.org/10.1029/2005PA001163>
- Kennett, J. P., & Stott, L. D. (1991). Abrupt deep-sea warming, paleoceanographic changes and benthic extinctions at the end of the Palaeocene. *Nature*, 353(6341), 225–229. <https://doi.org/10.1038/353225a0>
- Kirtland Turner, S., Hull, P. M., Kump, L. R., & Ridgwell, A. (2017). A probabilistic assessment of the rapidity of PETM onset. *Nature Communications*, 8, 353. <https://doi.org/10.1038/s41467-017-00292-2>
- Koch, P. L., Zachos, J. C., & Gingerich, P. D. (1992). Correlation between isotope records in marine and continental carbon reservoirs near the Palaeocene/Eocene boundary. *Nature*, 358(6384), 319–322. <https://doi.org/10.1038/358319a0>

- Kocken, I. J., Cramwinckel, M. J., Zeebe, R. E., Middelburg, J. J., & Sluijs, A. (2019). The 405 kyr and 2.4 Myr eccentricity components in Cenozoic carbon isotope records. *Climate of the Past*, *15*(1), 91–104. <https://doi.org/10.5194/cp-15-91-2019>
- Köhler-Rink, S., & Kühl, M. (2005). The chemical microenvironment of the symbiotic planktonic foraminifer *Orbulina universa*. *Marine Biology Research*, *1*(1), 68–78. <https://doi.org/10.1080/17451000510019015>
- Kominz, M. A., Browning, J. V., Miller, K. G., Sugarman, P. J., Mizintseva, S., & Scotese, C. R. (2008). Late Cretaceous to Miocene sea-level estimates from the New Jersey and Delaware coastal plain coreholes: An error analysis. *Basin Research*, *20*(2), 211–226. <https://doi.org/10.1111/j.1365-2117.2008.00354.x>
- Lear, C. H. (2000). Cenozoic deep-sea temperatures and global ice volumes from Mg/Ca in benthic foraminiferal calcite. *Science*, *287*(5451), 269–272. <https://doi.org/10.1126/science.287.5451.269>
- Lyle, M. W., Olivarez, A., Backman, J., & Tripathi, A. K. (2005). Biogenic sedimentation in the Eocene equatorial Pacific—The stuttering greenhouse and Eocene carbonate compensation depth. In P. A. Wilson, M. Lyle, & J. V. Firth (Eds.), *Proceedings of the Ocean Drilling Program, 199 Scientific Results* (Vol. 199, pp. 1–35 [Online]). College Station, TX: Ocean Drilling Program. Retrieved from. [http://www-odp.tamu.edu/publications/199\\_SR/199TOC.HTM](http://www-odp.tamu.edu/publications/199_SR/199TOC.HTM)
- Margolis, S. V., & Kennett, J. P. (1970). Antarctic glaciation during the tertiary recorded in sub-Antarctic deep-sea cores. *Science*, *170*(3962), 1085–1087. <https://doi.org/10.1126/science.170.3962.1085>
- Martínez-Botí, M. A., Marino, G., Foster, G. L., Ziveri, P., Henehan, M. J., Rae, J. W. B., et al. (2015). Boron isotope evidence for oceanic carbon dioxide leakage during the last deglaciation. *Nature*, *518*(7538), 219–222. <https://doi.org/10.1038/nature14155>
- Millero, F. J., & Pierrot, D. (1998). A chemical equilibrium model for natural waters. *Aquatic Geochemistry*, *4*(1), 153–199. <https://doi.org/10.1023/A:1009656023546>
- Misra, S., & Froelich, P. N. (2012). Lithium isotope history of Cenozoic seawater: Changes in silicate weathering and reverse weathering. *Science*, *335*(6070), 818–823. <https://doi.org/10.1126/science.1214697>
- Moebius, I., Friedrich, O., Edgar, K. M., & Sexton, P. F. (2015). Episodes of intensified biological productivity in the subtropical Atlantic Ocean during the termination of the Middle Eocene Climatic Optimum (MECO): Intensified productivity during the MECO. *Paleoceanography*, *30*, 1041–1058. <https://doi.org/10.1002/2014PA002673>
- Moore, T. C., Jarrard, R. D., Olivarez Lyle, A., & Lyle, M. (2008). Eocene biogenic silica accumulation rates at the Pacific equatorial divergence zone. *Paleoceanography*, *23*, PA2202. <https://doi.org/10.1029/2007PA001514>
- Myhre, G., Highwood, E., Shine, K., & Stordal, F. (1998). New estimates of radiative forcing due to well mixed greenhouse gases. *Geophysical Research Letters*, *25*(14), 2715–2718. <https://doi.org/10.1029/98GL01908>
- Norris, R. D., Wilson, D., Blum, P., & the Expedition 342 Scientists (Eds) (2014). *Proceedings of the Integrated Ocean Drilling Program, 342 Initial Reports*, (Vol. 342). College Station, TX: Ocean Drilling Program. Retrieved from. <http://publications.iodp.org/proceedings/342/342title.htm>
- Okai, T., Suzuki, A., Kawahata, H., Terashima, S., & Imai, N. (2002). Preparation of a new geological survey of Japan geochemical reference material: Coral JcP-1. *Geostandards Newsletter*, *26*(1), 95–99. <https://doi.org/10.1111/j.1751-908X.2002.tb00627.x>
- Pälike, H., Lyle, M. W., Nishi, H., Raffi, I., Ridgwell, A., Gamage, K., et al. (2012). A Cenozoic record of the equatorial Pacific carbonate compensation depth. *Nature*, *488*(7413), 609–614. <https://doi.org/10.1038/nature11360>
- Pearson, P. N., Ditchfield, P. W., Singano, J., Harcourt-Brown, K. G., Nicholas, C. J., Olsson, R. K., et al. (2001). Warm tropical sea surface temperatures in the Late Cretaceous and Eocene epochs. *Nature*, *413*(6855), 481–487. <https://doi.org/10.1038/35097000>
- Pearson, P. N., Foster, G. L., & Wade, B. S. (2009). Atmospheric carbon dioxide through the Eocene–Oligocene climate transition. *Nature*, *461*(7267), 1110–1113. <https://doi.org/10.1038/nature08447>
- Pearson, P. N., Olsson, R. K., Huber, B. T., Hemleben, C., & Berggren, W. A. (Eds) (2006). *Atlas of Eocene planktonic foraminifera*. Fredericksburg, USA: Cushman Foundation.
- Pearson, P. N., & Palmer, M. R. (1999). Middle Eocene seawater pH and atmospheric carbon dioxide concentrations. *Science*, *284*(5421), 1824–1826. <https://doi.org/10.1126/science.284.5421.1824>
- Pearson, P. N., & Palmer, M. R. (2000). Atmospheric carbon dioxide concentrations over the past 60 million years. *Nature*, *406*(6797), 695–699. <https://doi.org/10.1038/35021000>
- Pearson, P. N., Shackleton, N. J., & Hall, M. A. (1993). Stable isotope paleoecology of middle Eocene planktonic foraminifera and multi-species isotope stratigraphy, DSDP Site 523, South Atlantic. *The Journal of Foraminiferal Research*, *23*(2), 123–140. <https://doi.org/10.2113/gsjfr.23.2.123>
- Pekar, S. F., Hucks, A., Fuller, M., & Li, S. (2005). Glacioeustatic changes in the early and middle Eocene (51–42 Ma): Shallow-water stratigraphy from ODP Leg 189 Site 1171 (South Tasman Rise) and deep-sea  $\delta^{18}\text{O}$  records. *Geological Society of America Bulletin*, *117*(7), 1081–1093. <https://doi.org/10.1130/B25486.1>
- Penman, D. E. (2016). Silicate weathering and North Atlantic silica burial during the Paleocene–Eocene thermal maximum. *Geology*, *44*(9), 731–734. <https://doi.org/10.1130/G37704.1>
- Penman, D. E., Keller, A., D’Haenens, S., Kirtland Turner, S., & Hull, P. M. (2019). Atlantic deep-sea cherts associated with Eocene hyperthermal events. *Paleoceanography and Paleoclimatology*, *34*(2), 287–299. <https://doi.org/10.1029/2018PA003503>
- Penman, D. E., Turner, S. K., Sexton, P. F., Norris, R. D., Dickson, A. J., Boullia, S., et al. (2016). An abyssal carbonate compensation depth overshoot in the aftermath of the Palaeocene–Eocene thermal maximum. *Nature Geoscience*, *9*(8), 575–580. <https://doi.org/10.1038/ngeo2757>
- Penman, D. E., & Zachos, J. C. (2018). New constraints on massive carbon release and recovery processes during the Paleocene–Eocene thermal maximum. *Environmental Research Letters*, *13*, 105008. <https://doi.org/10.1088/1748-9326/aae285>
- Pisias, N. G., & Mix, A. C. (1988). Aliasing of the geological record and the search for long-period Milankovitch cycles. *Paleoceanography*, *3*(5), 613–619. <https://doi.org/10.1029/PA003i005p00613>
- Pomar, L., Baceta, J. I., Hallock, P., Mateu-Vicens, G., & Basso, D. (2017). Reef building and carbonate production modes in the west-central Tethys during the Cenozoic. *Marine and Petroleum Geology*, *83*, 261–304. <https://doi.org/10.1016/j.marpetgeo.2017.03.015>
- Premoli Silva, I., Wade, B. S., & Pearson, P. N. (2006). Taxonomy of Globigerinatheka and Orbulinoides. In P. N. Pearson, R. K. Olsson, B. T. Huber, C. Hemleben, & W. A. Berggren (Eds.), *Atlas of Eocene planktonic foraminifera* (pp. 461–508). Fredericksburg, VA: Cushman Foundation.
- Rae, J. W. B., Foster, G. L., Schmidt, D. N., & Elliott, T. (2011). Boron isotopes and B/Ca in benthic foraminifera: Proxies for the deep ocean carbonate system. *Earth and Planetary Science Letters*, *302*(3–4), 403–413. <https://doi.org/10.1016/j.epsl.2010.12.034>

- Roberts, J., Kaczmarek, K., Langer, G., Skinner, L. C., Bijma, J., Bradbury, H., et al. (2018). Lithium isotopic composition of benthic foraminifera: A new proxy for paleo-pH reconstruction. *Geochimica et Cosmochimica Acta*, 236, 336–350. <https://doi.org/10.1016/j.gca.2018.02.038>
- Rohling, E., & Members, P. P. (2012). Making sense of palaeoclimate sensitivity. *Nature*, 491(7426), 683–691. <https://doi.org/10.1038/nature11574>
- Rose, K. C., Ferraccioli, F., Jamieson, S. S. R., Bell, R. E., Corr, H., Creyts, T. T., et al. (2013). Early East Antarctic ice sheet growth recorded in the landscape of the Gamburtsev Subglacial Mountains. *Earth and Planetary Science Letters*, 375, 1–12. <https://doi.org/10.1016/j.epsl.2013.03.053>
- Sauermilch, I., Whittaker, J. M., Bijl, P. K., Totterdell, J. M., & Jokat, W. (2019). Tectonic, oceanographic, and climatic controls on the Cretaceous-Cenozoic sedimentary record of the Australian-Antarctic Basin. *Journal of Geophysical Research: Solid Earth*, 124, 7699–7724. <https://doi.org/10.1029/2018JB016683>
- Savian, J. F., Jovane, L., Giorgioni, M., Iacoviello, F., Rodelli, D., Roberts, A. P., et al. (2016). Environmental magnetic implications of magnetofossil occurrence during the Middle Eocene Climatic Optimum (MECO) in pelagic sediments from the equatorial Indian Ocean. *Paleogeography, Palaeoclimatology, Palaeoecology*, 441, 212–222. <https://doi.org/10.1016/j.palaeo.2015.06.029>
- Scher, H. D., Bohaty, S. M., Smith, B. W., & Munn, G. H. (2014). Isotopic interrogation of a suspected late Eocene glaciation: Hidden glaciation revealed in the Eocene. *Paleoceanography*, 29, 628–644. <https://doi.org/10.1002/2014PA002648>
- Scher, H. D., & Delaney, M. L. (2010). Breaking the glass ceiling for high resolution Nd isotope records in early Cenozoic paleoceanography. *Chemical Geology*, 269(3–4), 329–338. <https://doi.org/10.1016/j.chemgeo.2009.10.007>
- Sexton, P. F., Norris, R. D., Wilson, P. A., Pälike, H., Westerhold, T., Röhl, U., et al. (2011). Eocene global warming events driven by ventilation of oceanic dissolved organic carbon. *Nature*, 471(7338), 349–352. <https://doi.org/10.1038/nature09826>
- Sexton, P. F., Wilson, P. A., & Norris, R. D. (2006). Testing the Cenozoic multisite composite  $\delta^{18}\text{O}$  and  $\delta^{13}\text{C}$  curves: New monospecific Eocene records from a single locality, Demerara Rise (Ocean Drilling Program Leg 207). *Paleoceanography*, 21, PA2019. <https://doi.org/10.1029/2005PA001253>
- Sexton, P. F., Wilson, P. A., & Pearson, P. N. (2006a). Microstructural and geochemical perspectives on planktic foraminiferal preservation: “Glassy” versus “Frosty.”. *Geochemistry, Geophysics, Geosystems*, 7, Q12P19. <https://doi.org/10.1029/2006GC001291>
- Sexton, P. F., Wilson, P. A., & Pearson, P. N. (2006b). Palaeoecology of late middle Eocene planktic foraminifera and evolutionary implications. *Marine Micropaleontology*, 60(1), 1–16. <https://doi.org/10.1016/j.marmicro.2006.02.006>
- Shipboard Scientific Party (1988). Site 702. In P. F. Ciesielski, Y. Kristoffersen, et al. (Eds.), *Proceedings of the Ocean Drilling Program, 114 Initial Reports* (Vol. 114, pp. 483–548). College Station, TX: Ocean Drilling Program. Retrieved from [http://www-odp.tamu.edu/publications/114\\_IR/114TOC.HTM](http://www-odp.tamu.edu/publications/114_IR/114TOC.HTM)
- Shipboard Scientific Party (2004a). Site 1260. In J. Erbacher, D. C. Mosher, M. J. Malone, et al. (Eds.), *Proceedings of the Ocean Drilling Program, 207 Initial Reports* (Vol. 207, pp. 1–113). College Station, TX: Ocean Drilling Program. <https://doi.org/10.2973/odp.proc.ir.207.107.2004>
- Shipboard Scientific Party (2004b). Site 1263. In J. C. Zachos, D. Kroon, P. Blum, et al. (Eds.), *Proceedings of the Ocean Drilling Program, 208 Initial Reports* (Vol. 208, pp. 1–87). College Station, TX: Ocean Drilling Program. <https://doi.org/10.2973/odp.proc.ir.208.104.2004>
- Sluijs, A., Zeebe, R. E., Bijl, P. K., & Bohaty, S. M. (2013). A middle Eocene carbon cycle conundrum. *Nature Geoscience*, 6(6), 429–434. <https://doi.org/10.1038/ngeo1807>
- Somme, T. O., Helland-Hansen, W., & Granjeon, D. (2009). Impact of eustatic amplitude variations on shelf morphology, sediment dispersal, and sequence stratigraphic interpretation: Icehouse versus greenhouse systems. *Geology*, 37(7), 587–590. <https://doi.org/10.1130/G25511A.1>
- Spero, H. J., Lerche, I., & Williams, D. F. (1991). Opening the carbon isotope “vital effect” black box, 2, quantitative model for interpreting foraminiferal carbon isotope data. *Paleoceanography*, 6(6), 639–655. <https://doi.org/10.1029/91PA02022>
- Spofforth, D. J. A., Agnini, C., Pälike, H., Rio, D., Fornaciari, E., Giusberti, L., et al. (2010). Organic carbon burial following the middle Eocene climatic optimum in the central western Tethys. *Paleoceanography*, 25, PA3210. <https://doi.org/10.1029/2009PA001738>
- Stickley, C. E., St John, K., Koç, N., Jordan, R. W., Passchier, S., Pearce, R. B., & Kearns, L. E. (2009). Evidence for middle Eocene Arctic Sea ice from diatoms and ice-rafted debris. *Nature*, 460(7253), 376–379. <https://doi.org/10.1038/nature08163>
- Storey, M., Duncan, R. A., & Swisher, C. C. (2007). Paleocene-Eocene thermal maximum and the opening of the Northeast Atlantic. *Science*, 316(5824), 587–589. <https://doi.org/10.1126/science.1135274>
- Svensen, H., Planke, S., Malthes-Sørensen, A., Jamtveit, B., Myklebust, R., Rasmussen Eidem, T., & Rey, S. S. (2004). Release of methane from a volcanic basin as a mechanism for initial Eocene global warming. *Nature*, 429(6991), 542–545. <https://doi.org/10.1038/nature02566>
- Torres, M. A., Moosdorf, N., Hartmann, J., Adkins, J. F., & West, A. J. (2017). Glacial weathering, sulfide oxidation, and global carbon cycle feedbacks. *Proceedings of the National Academy of Sciences*, 114(33), 8716–8721. <https://doi.org/10.1073/pnas.1702953114>
- Tripati, A. K., Backman, J., Elderfield, H., & Ferretti, P. (2005). Eocene bipolar glaciation associated with global carbon cycle changes. *Nature*, 436(7049), 341–346. <https://doi.org/10.1038/nature03874>
- Tripati, A. K., Eagle, R. A., Morton, A., Dowdeswell, J. A., Atkinson, K. L., Bahé, Y., et al. (2008). Evidence for glaciation in the Northern Hemisphere back to 44 Ma from ice-rafted debris in the Greenland Sea. *Earth and Planetary Science Letters*, 265(1–2), 112–122. <https://doi.org/10.1016/j.epsl.2007.09.045>
- Vahlenkamp, M., Niezgodzki, I., De Vleeschouwer, D., Bickert, T., Harper, D., Kirtland Turner, S., et al. (2018). Astronomically paced changes in deep-water circulation in the western North Atlantic during the middle Eocene. *Earth and Planetary Science Letters*, 484, 329–340. <https://doi.org/10.1016/j.epsl.2017.12.016>
- van der Ploeg, R., Selby, D., Cramwinckel, M. J., Li, Y., Bohaty, S. M., Middelburg, J. J., & Sluijs, A. (2018). Middle Eocene greenhouse warming facilitated by diminished weathering feedback. *Nature Communications*, 9, 2877. <https://doi.org/10.1038/s41467-018-05104-9>
- van Hinsbergen, D. J. J., de Groot, L. V., van Schaik, S. J., Spakman, W., Bijl, P. K., Sluijs, A., et al. (2015). A paleolatitude calculator for paleoclimate studies. *PLoS ONE*, 10, e0126946. <https://doi.org/10.1371/journal.pone.0126946>
- Vigier, N., & Goddérís, Y. (2015). A new approach for modeling Cenozoic oceanic lithium isotope paleo-variations: The key role of climate. *Climate of the Past*, 11(4), 635–645. <https://doi.org/10.5194/cp-11-635-2015>
- Vigier, N., Rollion-Bard, C., Levenson, Y., & Erez, J. (2015). Lithium isotopes in foraminifera shells as a novel proxy for the ocean dissolved inorganic carbon (DIC). *Comptes Rendus Geoscience*, 347(1), 43–51. <https://doi.org/10.1016/j.crte.2014.12.001>
- Wade, B. S., Al-Sabouni, N., Hemleben, C., & Kroon, D. (2008). Symbiont bleaching in fossil planktonic foraminifera. *Evolutionary Ecology*, 22(2), 253–265. <https://doi.org/10.1007/s10682-007-9176-6>

- Westerhold, T., & Röhl, U. (2013). Orbital pacing of Eocene climate during the Middle Eocene Climate Optimum and the chron C19r event: Missing link found in the tropical western Atlantic: Orbital pacing of Eocene climate. *Geochemistry, Geophysics, Geosystems*, *14*, 4811–4825. <https://doi.org/10.1002/ggge.20293>
- Westerhold, T., Röhl, U., Donner, B., Frederichs, T., Kordesch, W. E. C., Bohaty, S. M., et al. (2018). Late Lutetian thermal maximum-crossing a thermal threshold in Earth's climate system? *Geochemistry, Geophysics, Geosystems*, *19*, 73–82. <https://doi.org/10.1002/2017GC007240>
- Westerhold, T., Röhl, U., Donner, B., & Zachos, J. C. (2018). Global extent of early Eocene hyperthermal events: A new Pacific benthic foraminiferal isotope record from Shatsky Rise (ODP Site 1209). *Paleoceanography and Paleoclimatology*, *33*(6), 626–642. <https://doi.org/10.1029/2017PA003306>
- Westerhold, T., Röhl, U., Pälike, H., Wilkens, R., Wilson, P. A., & Acton, G. (2014). Orbitally tuned timescale and astronomical forcing in the middle Eocene to early Oligocene. *Climate of the Past*, *10*(3), 955–973. <https://doi.org/10.5194/cp-10-955-2014>
- Witkowski, J., Bohaty, S. M., Edgar, K. M., & Harwood, D. M. (2014). Rapid fluctuations in mid-latitude siliceous plankton production during the Middle Eocene Climatic Optimum (ODP Site 1051, western North Atlantic). *Marine Micropaleontology*, *106*, 110–129. <https://doi.org/10.1016/j.marmicro.2014.01.001>
- Witkowski, J., Bohaty, S. M., McCartney, K., & Harwood, D. M. (2012). Enhanced siliceous plankton productivity in response to middle Eocene warming at Southern Ocean ODP Sites 748 and 749. *Palaeogeography, Palaeoclimatology, Palaeoecology*, *326–328*, 78–94. <https://doi.org/10.1016/j.palaeo.2012.02.006>
- Zachos, J. C., Rohl, U., Schellenberg, S. A., Sluijs, A., Hodell, D. A., Kelly, D. C., et al. (2005). Rapid acidification of the ocean during the Paleocene-Eocene thermal maximum. *Science*, *308*(5728), 1611–1615. <https://doi.org/10.1126/science.1109004>
- Zeebe, R. E. (2012). LOSCAR: Long-term Ocean-atmosphere-Sediment Carbon cycle Reservoir Model v2.0.4. *Geoscientific Model Development*, *5*(1), 149–166. <https://doi.org/10.5194/gmd-5-149-2012>
- Zeebe, R. E., & Wolf-Gladrow, D. A. (2001). *CO<sub>2</sub> in seawater: Equilibrium, Kinetics, Isotopes*. Amsterdam: Elsevier.
- Zeebe, R. E., Wolf-Gladrow, D. A., Bijma, J., & Hönisch, B. (2003). Vital effects in foraminifera do not compromise the use of  $\delta^{11}\text{B}$  as a paleo-*p* H indicator: Evidence from modeling: Cretaceous marine temperature evolution. *Paleoceanography*, *18*(2), 1043. <https://doi.org/10.1029/2003PA000881>

## References From the Supporting Information

- Cameron, A. C., Gelbach, J. B., & Miller, D. L. (2008). Bootstrap-based improvements for inference with clustered errors. *Review of Economics and Statistics*, *90*(3), 414–427. <https://doi.org/10.1162/rest.90.3.414>
- Liu, R. Y. (1988). Bootstrap procedures under some non-iid models. *The Annals of Statistics*, *16*(4), 1696–1708.
- Mammen, E. (1993). Bootstrap and wild bootstrap for high dimensional linear models. *The Annals of Statistics*, *21*(1), 255–285.

## Erratum

In the originally published version of this article, the author contributions were listed incorrectly due to a rendering error. The error has since been corrected and this version may be considered the authoritative version of record.